NASA CONTRACTOR REPORT

NASA CR-7

NASA CR-783

RESEARCH ON A NON-DESTRUCTIVE FLUIDIC STORAGE CONTROL DEVICE

by T. D. Reader and S. K. Ho

Prepared by
GIANNINI CONTROLS CORPORATION
Malvern, Pa.
for Electronics Research Center

NATIONAL AERONAUTICS AND SPACE ADMINISTRATION • WASHINGTON, D. C. • JUNE 1967

NASA CR-783

RESEARCH ON A NON-DESTRUCTIVE FLUIDIC STORAGE CONTROL DEVICE

By T. D. Reader and S. K. Ho

Prepared under Contract No. NAS 12-43 by
GIANNINI CONTROLS CORPORATION
Malvern, Pa.

for Electronics Research Center

NATIONAL AERONAUTICS AND SPACE ADMINISTRATION

For sale by the Clearinghouse for Federal Scientific and Technical Information
Springfield, Virginia 22151 – CFSTI price $3.00

ABSTRACT

This report describes a non-destructive fluidic memory device with associated fluidic alphanumeric display, developed by Giannini Controls Corporation under contract NAS 12-43 with NASA Electronics Research Center. The device uses the surface tension of a liquid bead in an hour-glass-shaped cavity to achieve a bi-stable memory effect which does not require a continuous supply of fluid power. Thus, the storage device may be left passive for years without losing its information, yet the information may be changed at any time by means of a control signal. We have shown that this new approach to a fluidic memory can be easily mated to conventional fluidic devices, and that a useful fluidic display is also feasible.

It appears that the non-destructive fluidic storage device is the forerunner of a whole new technology ranging from infinite impedance analog devices to electro-fluidic transducers. Its successful development is a major contribution to the field of fluidics.

TABLE OF CONTENTS

LIST OF FIGURES

SYMBOLOGY

A,B,C,D,E	Columns of cells in the display unit or Boolean symbols
a	Acceleration of fluid particles at a given cross section
a,b,c,d,e,f,g	Rows of cells in the display unit
b	Core width
b_o	Throat nozzle width
d_o	Perpendicular Distance between nozzles and receivers
E_c	Energy at nozzle
f	Boolean Function
F	Force tending to break bead
F_{st}	Force due to surface tension
h	Ratio : Z_{in}/Z_1
k	Z_1/Z_2
m	Mass
P	Bead internal pressure
P_a	Pressure in right cell
P_b	Bias pressure
P_A, P_B, P_C	Input pressures to AND gates
P_c	Control pressure
P_{in}	Sensing pressure supply
P_{oL}	Left side output pressure
P_{oR}	Right side output pressure
P_s	Supply pressure
P_{sn}	Sensing pressure
P_{sw}	Switching pressure

P_{s1}, P_{s0}	Sensing pressures in "1" and "0" states
Q	Volumetric rate of flow
Q_o	Flow at nozzle
R,r	Radius of memory cell and switching path
S	Sensing hole
sw	Switch
t	Time
v	Velocity of fluid
V_4	Center line velocity
V_o	Original nozzle velocity
w_o	Receiver Width
x	Axial distance measured from nozzle
x_o	Length of transition zone
y	Distance from jet center line
Y	Effective value of y
Z	Impedance
Z_a	$(Z_1 + Z_2)/(Z_1 + Z_2 + Z_L)$
Z_b	$Z_1 Z_L/(Z_1 + Z_L)$
Z_{in}	Input series impedance
Z_L	Input impedance of amplifier
θ	Cone angle between wall of cavity and axis of revolution
Φ_c	Contact angle
α	Angle between direction of surface forces and axis of chamber
$\sim$	Resistance
η	Surface tension
δ	k/1 + k

INTRODUCTION

Fluidic technology has advanced to the point where it is now possible to specify areas where it may be applied to advantage. These areas include:

1. Digital
   a. general counting and industrial sequencing controls
   b. simple logic functions involving switching circuits
   c. adding and calculating machines
   d. adaptive parallel logic computers
2. Analog
   a. multipliers, function generators, and general purpose analog computers
   b. petro-chemical and process control
   c. flight stabilization
   d. auto-pilots
   e. turbine speed control
   f. adaptive systems
3. Hybrid
   a. analog-to-digital and digital-to-analog converters
   b. adaptive systems whose characteristics are required to change incrementally
   c. adaptive systems designed to respond selectively to different stimuli

An area in which fluidic technology has been weak is the digital memory. The only memory device using fluids and no solid mechanical parts was a flip-flop based either on the Coanda effect or on an interconnecting of two NOR gates. In either case power was required to retain the data stored by the flip-flops. If all power were removed, the data would be lost.

Electronic computers had a similar problem when their chief means of storing data was either electronic or dynamic, since both electronic flip-flops and the dynamic mercury delay-line memory would lose their data when the machine was shut down. The magnetic core memory was an invention which permitted data to be stored regardless of whether the power to the machine was on or off, since the data stored was in the form of permanent magnetism. The magnetic polarity of a tiny ferrite "doughnut" was changed by means of

a "write" current passing through a wire threaded through it. Depending on the direction of the write current the core would store either a "1" or a "0". Reading was achieved by detecting the induced current in a wire resulting from writing a "0". If the information was already "0" there would be no induced current while if the information was a "1" there would be an induced current caused by the change in magnetic flux.

In fluidics there appeared to be no phenomena analogous to permanent magnetism, until the idea of utilizing surface tension was conceived at Giannini's Astromechanics Research Division. Using a small bead of a specially prepared liquid capable of assuming either of two stable positions within an "hourglass" shaped cavity, it has been found possible to store the data in a fluidic system even in the absence of power. The unique feature of this non-destructive storage device is the absence of any solid moving mechanical parts.

This report describes the work performed in the laboratory of the Astromechanics Research Division, under the direction of Mr. Trevor D. Reader. Mr. E. Hilborn, Control and Information Systems Laboratory of NASA, Electronics Research Center was the Government's Technical Monitor. The work covered an investigation of those two-phase systems found to display a non-destructive memory effect. Various combinations of materials were studied and several unique fluid bead approaches were discovered.

To illustrate its potential, the non-destructive memory was combined with a card reader, logic coding and decoding networks, and a fluidic alpha-numeric display. The final demonstration model shows that the non-destructive fluidic memory is easily mated with conventional digital fluidic devices, and that a useful display pattern can be achieved by means of fluidic concepts only.

I. GENERAL DESCRIPTION

The objective of this contract was to conceive, build, test, and evaluate a system of digital computation utilizing a non-destructive binary fluidic memory. Additionally, in order to demonstrate the non-destructive nature of the memory and its ability to do useful work, an alpha-numeric display was incorporated into the system. Figure 1 is a functional block diagram of the system consisting of a Memory Unit, a Decoding Matrix, and Encoding Matrix, and an Alpha-Numeric Display.

The Memory Unit contained three non-destructive fluidic bead elements. These elements could be "set" or "reset" by temporary insertion of a punched IBM card.

Sensing channels from the memory fed binary information to the Decoding Matrix which converted the three-bit-binary information into one of eight unique outputs.

Each of the eight outputs from the Decoding Matrix was then "fanned out" in the Encoding Matrix to give various combinations of thirty-five possible outputs. These outputs fed a 7 x 5 array of cells which comprised the Alpha-numeric Display Unit. Various combinations of the thirty-five inputs to this display unit permitted eight different alpha-numeric symbols to be presented.

The work under the contract was classified into three major areas.

1. The development of a mathematical foundation for the entire system. This included construction of a mathematical model of memory and logic elements, as well as the use of Boolean Algebra for logic circuit design.

2. The development of a Material Study which included a wide search of chemical systems exhibiting high surface tension; the liquids employed having low volatility, non-toxicity, and chemical stability.

3. The design of a fluidic interface between the non-destructive memory and a display panel. The work involved in this item included element design (such as memory and logic elements), low gain logic circuit amplifiers, integrated circuitry, display method, and system function.

These three areas were interdependent and therefore needed to be studied simultaneously. It was necessary to use the water table technique to design special "isolated" sensing amplifiers to sense the information in the memory cells. The logical designs of the decoding and encoding matrices were affected by the limitations in loading and fan-out capabilities of the fluidic

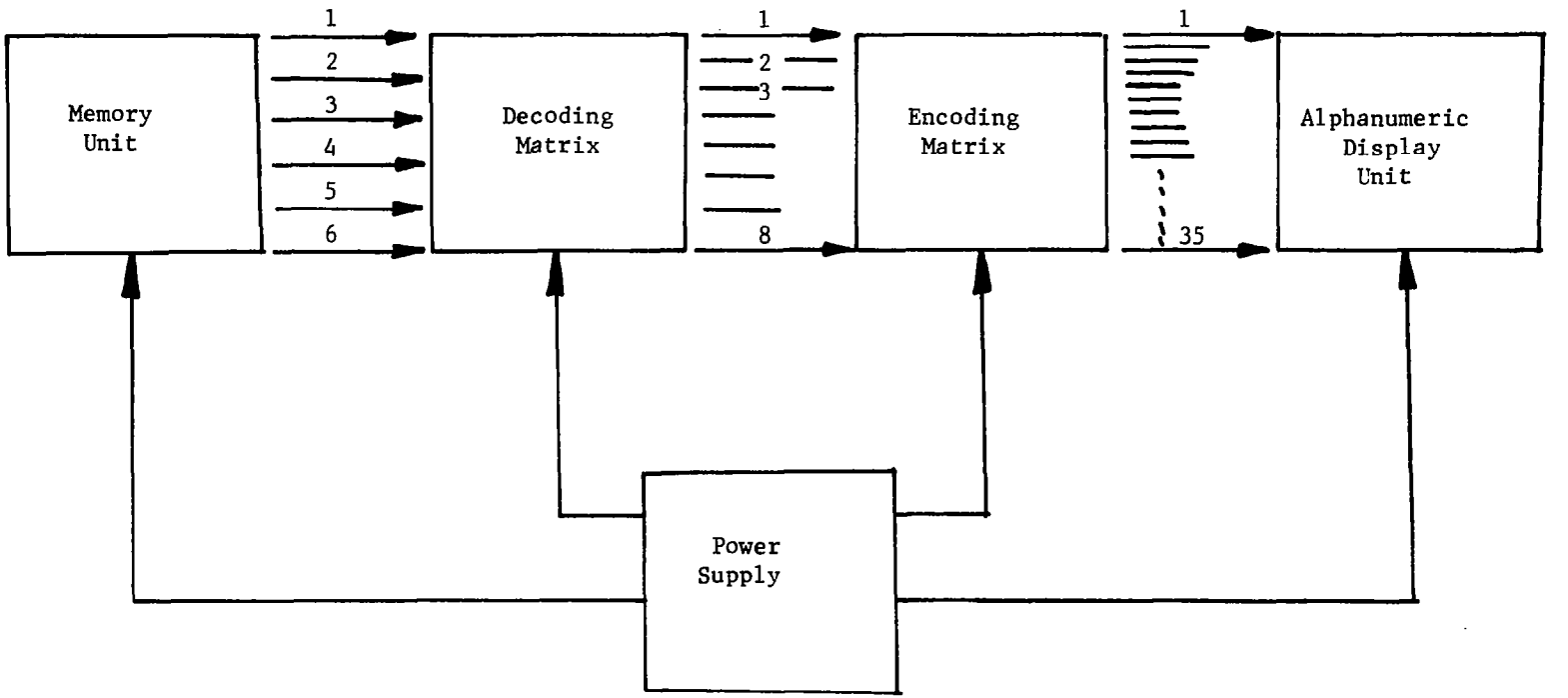

FIGURE 1 System Block Diagram

devices used. These devices were designed to ensure compatibility both with the non-destructive memory and with the display unit.

II. ELEMENT DESCRIPTION

2.1 Non-Destructive Memory

Theory. A fluid bead sits in a memory chamber as shown in Figure 2. When the bead is small (say 1/8" dia.) the surface tension causes it to become approximately spherical in shape. A pressure P_{sw} applied to the left side will switch the bead from the left to the right hand portion of the cell. Once the bead has been switched to the right it will stay there even if the power source is shut off. A similar procedure takes place when the bead is switched from the right side to the left. Thus the device acts as a flip-flop with non-destructive memory. P_{sn} is a constant pressure supply which senses the presence or absence of the fluid bead in the right hand chamber.

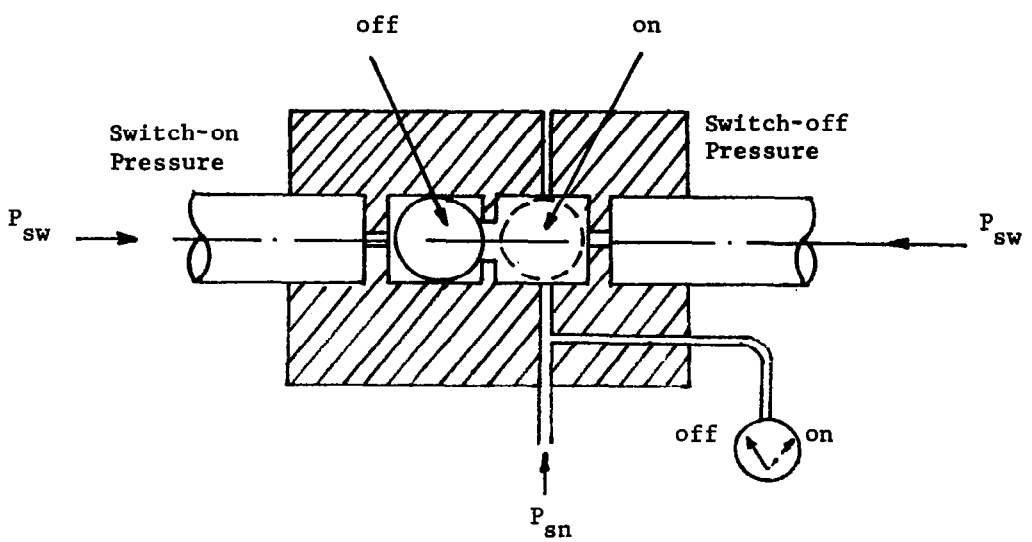

FIGURE 2 NON-DESTRUCTIVE MEMORY ELEMENT

An analysis of the forces involved when a bead of fluid is forced through a restriction is given in Appendix A. A study of the chemistry of fluid beads is reported in Appendix B.

Switching tests performed on elements based on the concept shown in Figure 2 revealed that the liquid bead had a tendency to

break up and plug the sensing holes after passing through the central orifice. Several different design concepts were tested, until it was found that a satisfactory "two-dimensional" design could be built using the pantograph milling machine. The problem of plugging the sensing holes was not solved until it became evident that the liquid bead should not be allowed to strike a wall after being squeezed through the neck of the cavity.

In order to provide a "rolling" action as the bead was switched across the restriction, an asymmetric design was investigated. By providing a continuous surface from one cavity to the other, the liquid bead was able to roll without shock, on being switched. Figure 3 shows the details of the final version of the non-destructive memory element. This version was incorporated in the final demonstration model.

2.2 Sensing Element

The function of the sensing element is to determine the side of the memory cell in which the mercury bead rests. Either an amplifier or an HDL-type discriminator can be used. There are two ways of sensing the mercury bead: 1) the use of the positive pressure sensing method or 2), the negative pressure sensing method. The first method is shown in Figure 4(a), in which a combination of a memory element and a sensitive amplifier is used. The amplifier has a bias P_b . When the fluid bead is in the "1" position, the sensing pressure, P_{sn}, that is applied to the memory element is also applied to the input of impedance Z_3. P_{sn} will be greater than P_b. Therefore, the amplifier will be in the "1" state. In the other case, when the mercury bead is in the "0" position, the sensing air will be divided into two paths. This lowers the pressure P_{sn}, and under these conditions P_{sn} produces a control pressure P_c which is below the value of P_b . Thus, the amplifier is allowed to return to its "0" state.

The second sensing method (which was the one selected for the demonstration model) is similar to the first, except that there is no externally applied sensing air. A memory cell with two sensing probes is connected to a HDL-type flip-flop discriminator as shown in Figure 4(b). When the mercury bead is in the "1" position, the corresponding control probe is blocked;

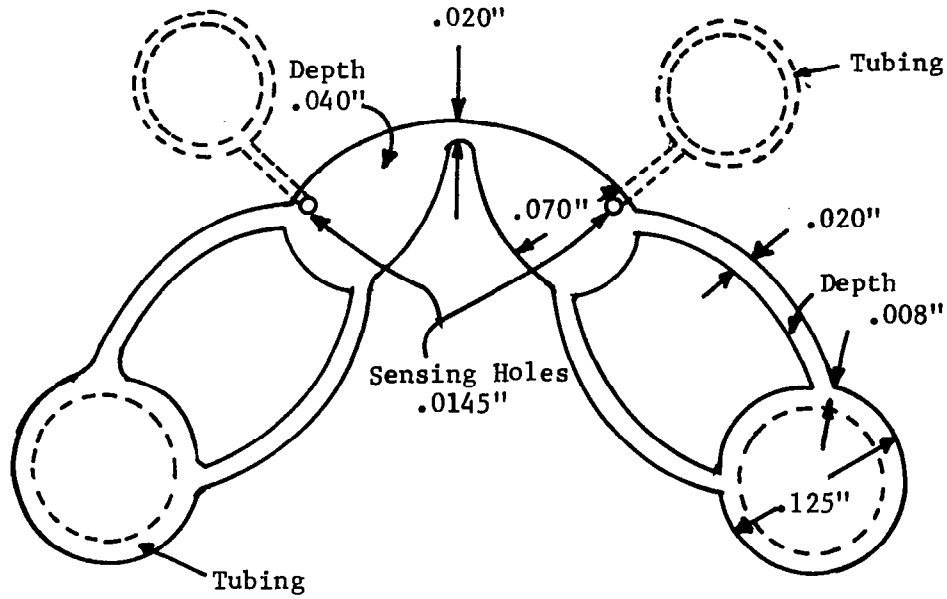

FIGURE 3 Final Version of Non-Destructive Memory Element

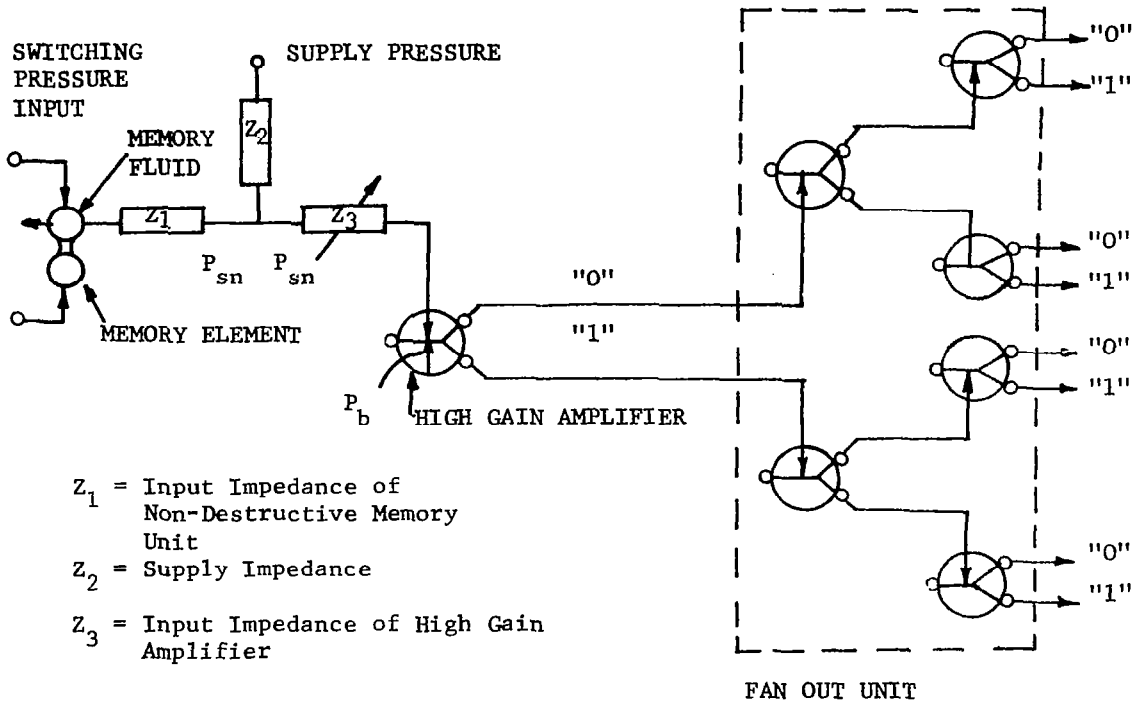

(a) POSITIVE SENSING

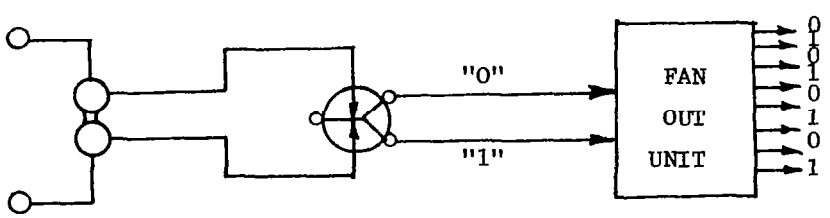

(b) NEGATIVE SENSING

FIGURE 4 Sensing Elements

therefore, the discriminator gives a "1" output. The same principle applies to the other side. The difficulty of the first method of sensing is that P_{sn} is very critical; it must be adjusted near P_b, and when supply pressure is changed, P_{sn} must be readjusted. The second method is independent of the variation of supply pressure to the discriminator; hence, it is more reliable in operation. The characteristic curves of the discriminator are shown in Figure 5. We notice that the pressure P_{sn} is actually negative; therefore, we name it the "negative sensing method". The discriminator gave an output of about 30% input supply pressure. In our system the output pressures were between 3 and 4 inches of water.

The output from each of the three sensing elements was fed into a cascade of "low gain" amplifiers. The function of these amplifiers was to drive the decoding logic net described previously.

2.3 Low Gain Amplifier

The definition of "gain" in this binary system is the pressure ratio between input and output when the control input is in the "ON" state. The average gain for typical loading conditions was 4. The control input and output relationship for the low gain digital amplifier is discussed in Appendix D. One important feature of the characteristic curves is that no hysteresis exists. Experience has shown non-hysteretic amplifiers to be faster and more reliable in operation than hysteretic amplifiers when used as logic devices in which the memory feature is not required.

2.4 AND Gate

The use of passive elements in fluidics has resulted in great simplification in logical design problems. The design of a passive AND gate is shown in Appendix D. Its principle of operation is that in order to obtain an output, two control jets must impinge at right angles to each other. A receiver is so placed that unless both control nozzles are supplying air, no air enters the receiver.

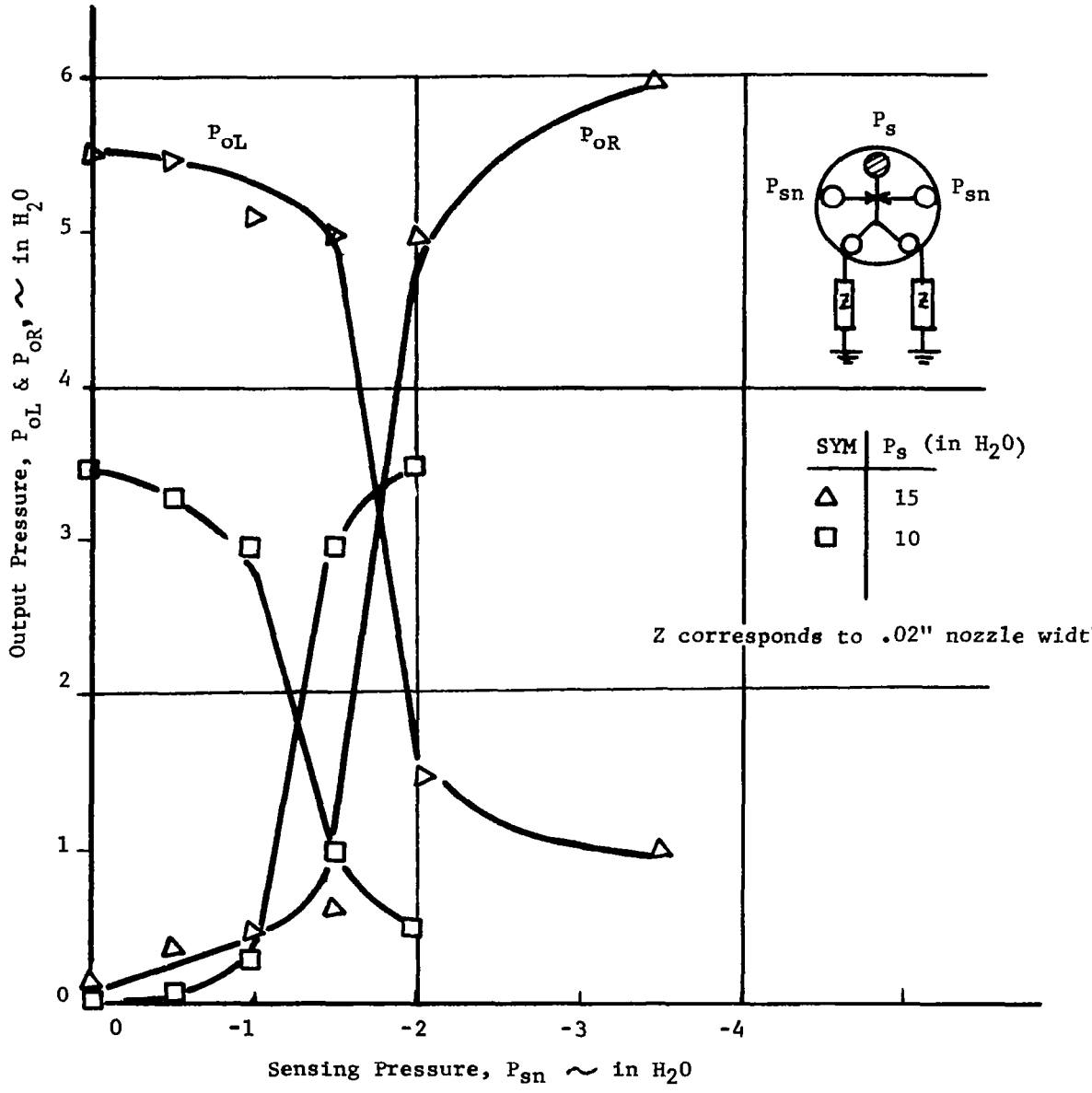

FIGURE 5 Memory Discriminator Characteristic Curve

2.5 OR Gate

Another passive element essential to the design of flip-flops using inverters is the OR gate. The design of a passive OR gate is shown in Appendix D . The operation of this element is different from that of the AND gate in that either control nozzle is capable of directing a jet of air at the receiver. Thus the OR gate produces an output when either or both control nozzles are supplying jets of air. An examination of the geometries of the AND gate and the OR gate illustrated in Appendix D will reveal graphically the difference between their modes of operation.

III. BREADBOARD MODEL

The function of the whole system is to read information from a punched card in order to store information in the non-destructive memory element and to display this information on a panel.

Figure 6(a) shows the prototype system block diagram. An IBM card reader reads the code punched in the IBM card(when the card is inserted into the slot) and stores the data in the memory elements. The information thus stored remains, even in the absence of power. Since there are three memory elements, three bits of information can be stored. In other words, a total of eight ($2^3 = 8$) different combinations, or eight different characters, can be displayed. Figure 6(b) is a photograph of the prototype system in breadboard form. Each unit is described in the following sections.

3.1 IBM Card Reader

The function of the IBM card reader is to transfer the binary coded information on the IBM card into the memory element. The function of the card reader can be described as a pneumatic switching circuit, as shown in the upper part of Figure 7. Switch #1 is a power switch which can be turned on and off by closing the hole S on the control port of a monostable flip-flop. When the IBM card is inserted fully into the card reader the hole S is blocked by the card and the power supply is turned on immediately. As soon as the card is pulled out, the switch opens again. This provides a reliable switching action that eliminates any false alarms which might take place during the insertion and removal of the IBM card in the card reader. Switches #2, #4, and #7 are equivalent to holes punched in an IBM card. There are three punched holes in each of the eight cards used with this system. This means that three corresponding switches are closed when the card is inserted in the card reader; for example, Figure 6 shows switches #2, #4, and #7 closed according to the specific code $\overline{A}\ \overline{B}\ C$.

3.2 Memory Unit

This unit consists of three non-destructive memory elements based on the design shown in Figure 3. These elements are ac-

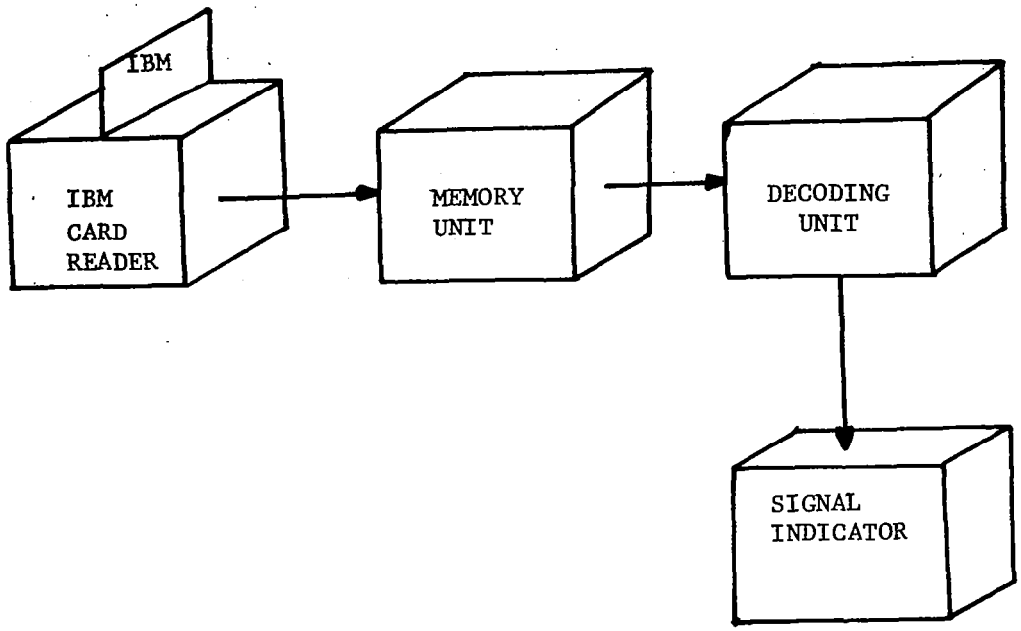

(a) Prototype System Block Diagram

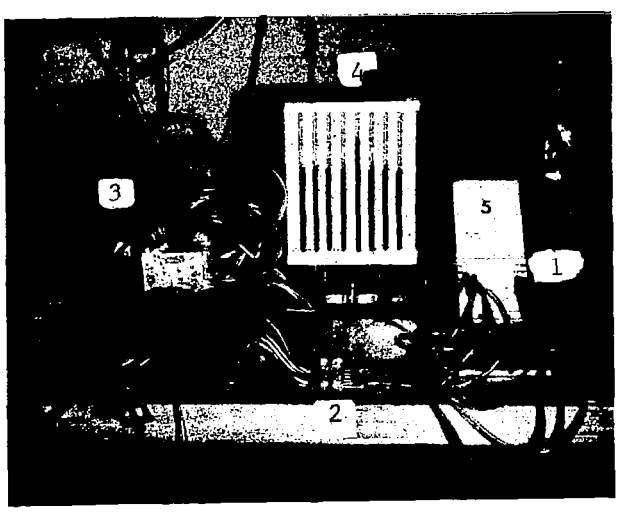

1. IBM Card Reader
2. Memory Unit
3. Decoding Unit
4. Signal Indicator

(b) Prototype System Breadboard Lay-Out

FIGURE 6

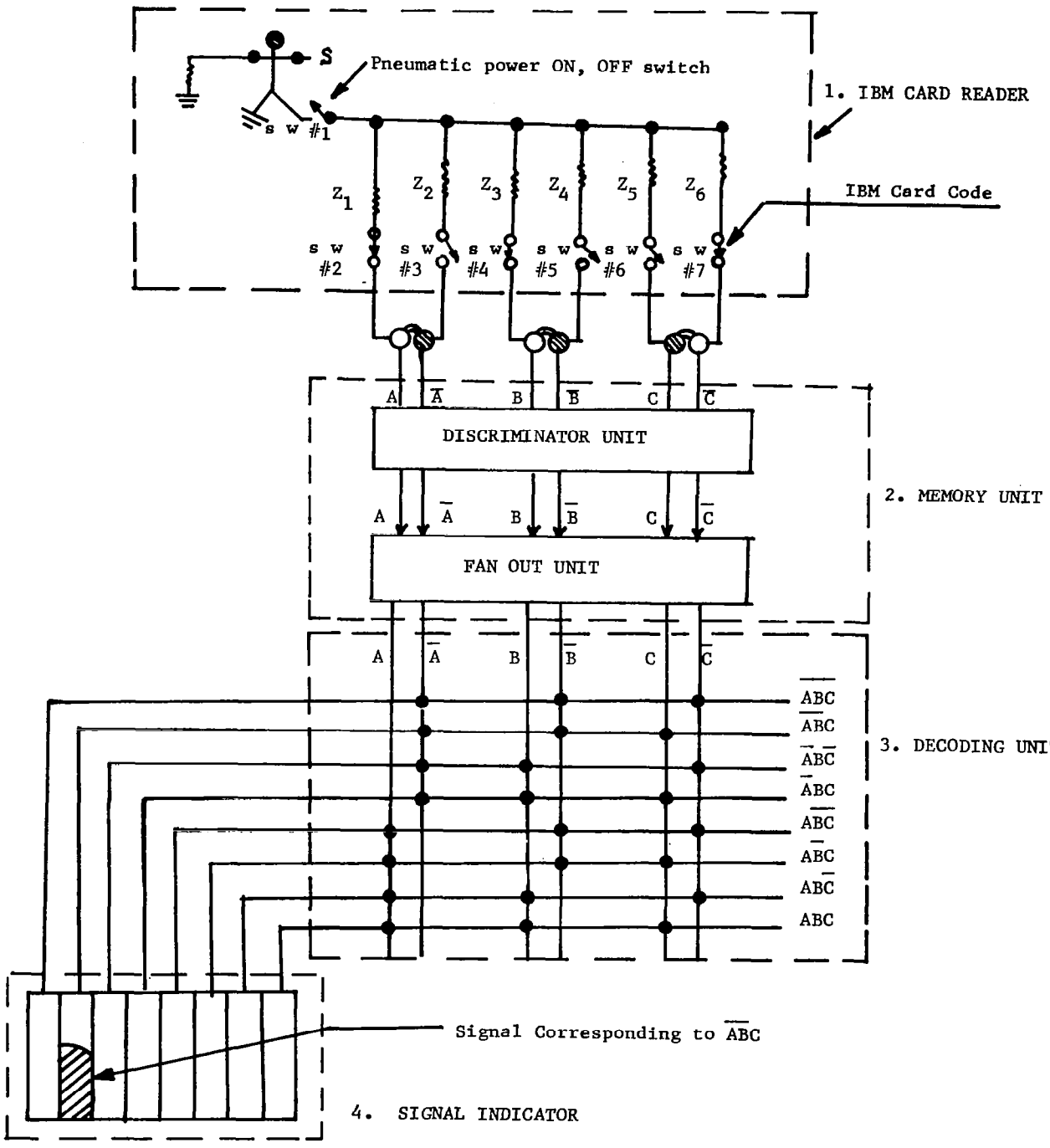

FIGURE 7 Prototype System Schematic Diagram

tuated only when a punched card has been inserted into its slot. Their states are sensed by discriminators whose outputs are fanned out in order to drive the decoding matrix. The details of the memory elements were described in section 2.1, and the flip-flop discriminators were described in section 2.2.

3.3 Decoding Unit

The logic used in this system is basically a decoding matrix, as shown in Figure 7 . The decoding matrix, made by eight AND logic elements, transforms the information stored inside the memory element into a signal which can be displayed on a signal indicator (for instance, a manometer, etc.). Each row of the decoding matrix corresponds to a specific item of stored information. For example, in Figure 7 a signal from the second row corresponds to $\bar{A}\ \bar{B}\ C$. The three black dots on each row of the decoding matrix represent inputs of an integrated logic block; for instance, the first row represents an integrated logic block with three inputs $\bar{A}\ \bar{B}$ and $\bar{C}$. This logic block forms the Boolean AND function on the three inputs. It supplies a signal output only when the $\bar{A}\ \bar{B}\ \bar{C}$ inputs are on simultaneously. Therefore the eight outputs of the decoding matrix are mutually exclusive.

3.4 Signal Indicator

The breadboard version of the demonstration model used the simple manometer-type indicator shown in Figure 6 (b). The eight manometer tubes were connected to the eight outputs of the decoding units and indicated which of the eight different combinations of memory settings had been selected by the card reader.

IV. FINAL DEMONSTRATION MODEL

4.1 Display Panel

The display panel for the final model consists of thirty-five deep cells covered by a translucent screen. Each cell contains an elastomer bead. When the bead is raised by air pressure from the logic circuit, it appears as a white spot beneath a translucent screen. A letter or number is formed when selected combinations of beads are raised. Each bead falls into the bottom of its cell once its signal has disappeared.

There are eight symbols: "A", "C", "D", "G", "R", "O", "5", "6", which were designed to be displayed on the panel. These symbols are shown in Figure 8(a) and were selected in a semi-random fashion as being typical of the 35-cell alpha-numeric system. In the design of the logic circuits the rows of cells in the display panel were designated by lower case letters a, b, c, d, e, f, and g; the columns were designated by upper case letters A, B, C, D, E as shown in Figure 8(b). In this way each cell could be represented by means of an upper and a lower case letter. Figure 8(c) shows the number of different symbols which require the use of each cell in the array. The logical design for the display is discussed in further detail in Appendix E. It should be noted that a 5 x 7 matrix of memory units with only one side exposed to view could have been used as the display unit, in which case information would have remained displayed even in the absence of power. The choice of elastomer beads was made because their implementation was simpler within the cost and manpower limitations of the contract.

4.2 Location of Key Elements

In order to facilitate access to the non-destructive memory elements, an adapter plate is provided which permits the memory elements to be plugged in without the need for disconnecting any tubing. Figure 9 shows the model with its cover raised. In this photograph the three memory elements may be seen to be close to the card reader slot near the front of the model.

The display panel is mounted in such a way that it may be removed without disturbing the other elements. Sufficient clearance between the sides of the model and the logic elements was allowed to facilitate removal and replacement of all components.

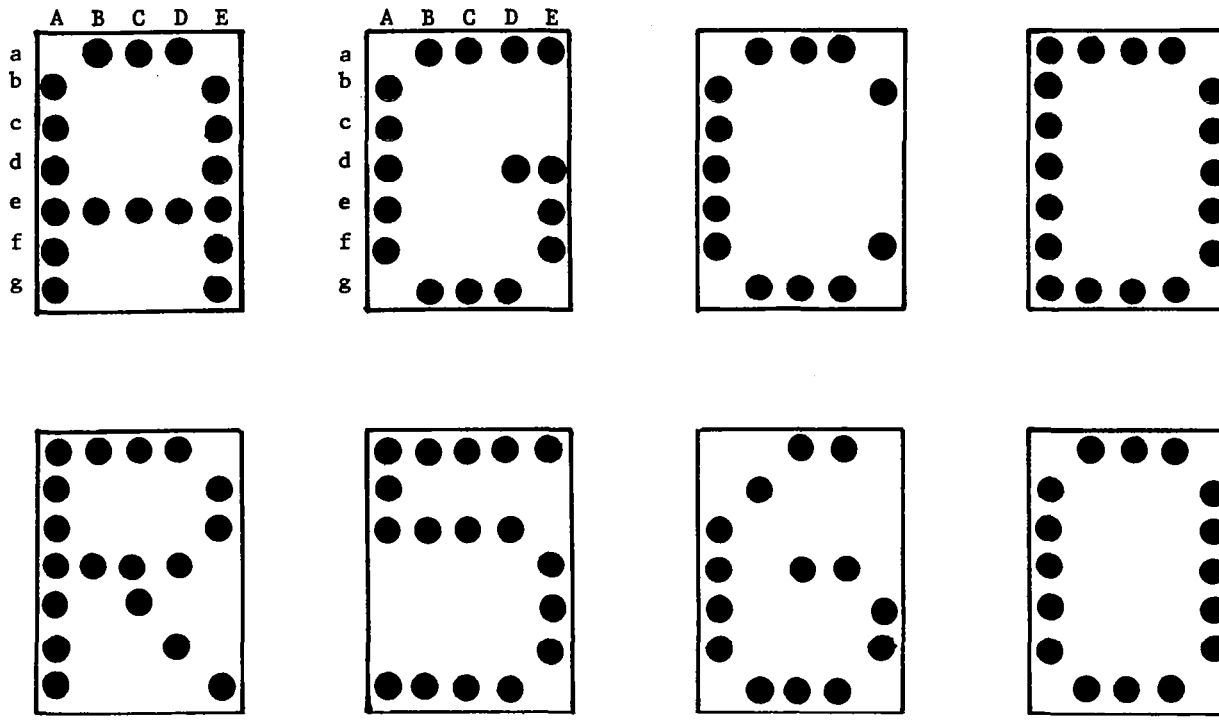

(a) Pattern of Display Symbols

DOT INDEX

Aa	Ba	Ca	Da	Ea
Ab	Bb	Cb	Db	Eb
Ac	Bc	Cc	Dc	Ec
Ad	Bd	Cd	Dd	Ed
Ae	Be	Ce	De	Df
Af	Bf	Cf	Df	Ef
Ag	Bg	Cg	Dg	Eg

(b) Display Panel Index

	A	B	C	D	E
a	3	7	8	8	2
b	7	1	0	0	5
c	8	1	1	1	4
d	7	1	2	3	5
e	7	1	2	1	6
f	7	0	0	1	7
g	4	6	6	6	2

(c) Display Panel Cell Loading

FIGURE 8

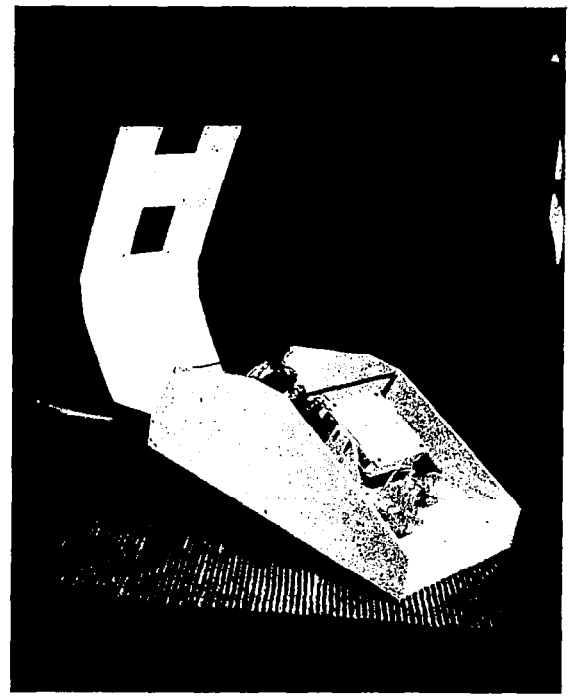

FIGURE 9 Demonstration Model with Cover Raised

4.3 Fabrication of the Final Model

Having demonstrated a breadboard version of the model, it was necessary to package the elements in a reasonably compact shell. In order to reduce the distance between the elements, and hence the quantity of plastic tubing, the brass power supply tubes of all active elements were plugged into a common manifold. The final model is a compact portable unit containing the IBM card reader, the non-destructive fluidic storage device, the encoding and decoding logic elements, and the display panel. Figure 10 is a photograph of the final model which was delivered to the NASA Electronics Research Center upon the completion of this phase of the program.

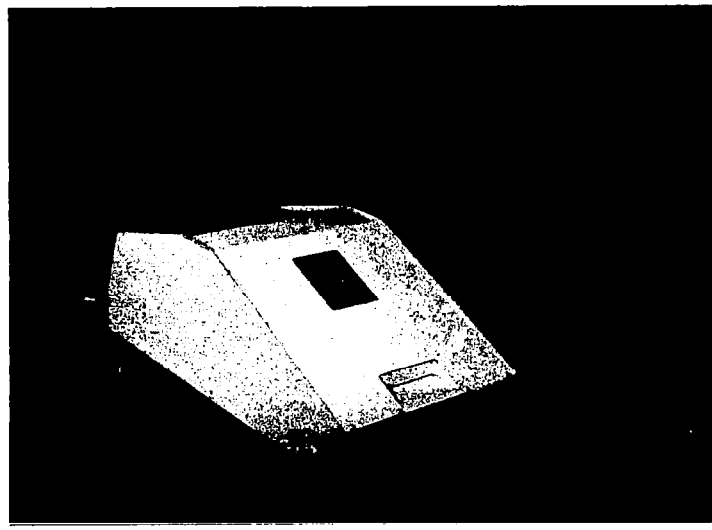

FIGURE 10 Demonstration Model

DEPTH 21 1/4"

WIDTH 10 1/2"

HEIGHT 7 3/4"

V. SYSTEM TEST

There were five factors to be considered in the system study:

1) load isolation
2) pressure stability of the system
3) mechanical response of the system
4) interference between the logic elements due to the bleed air
5) system debugging

5.1 Load Isolation

Isolation between stages was an important factor contributing to maximum power gain. In our amplifier, the deflection of the power jet was based upon the momentum exchange between the power jet and the control jet; hence, maximum power gain was desirable. To achieve the best impedance matching between stages, the input impedance (control port) of the element was designed to be equal to the output impedance of the previous stage. Nozzle width in all the elements was .02", while the aspect ratio was 2:1. Also, all elements were designed to work properly even under the poorest ("worst case") operating conditions; for instance, one output could have been fully loaded while the other was completely open. The design under the poorest conditions resulted in a very stable operation pressure range, and the isolation eliminated the feedback problem caused by different loads.

5.2 The Pressure Stability of the System

The excellent stability of the system was due to the two factors mentioned above, namely load isolation and impedance matching. It functions well between 12 to 15 inches of water supply pressure. The lower pressure limit was governed by the amplifier minimum operating pressure, and the upper limit was determined by the sensing discriminator output, as described early in section 2.2.

5.3 Mechanical Response of the System

Laboratory tests have shown that switching frequencies of up to 35 cycles per second can be obtained from a device employing a fluid bead measuring one sixteenth of an inch in diameter.

It has also been shown that the fluid bead memory device is capable of operating under mechanical vibration up to at least 3 g over the frequency range from 10 to 200 Hertz. A more detailed discussion of these results may be found in Appendix C.

5.4 Interference Between the Logic Elements Due to Bleed Air

Since not all the air ejected from the power nozzles of each element could be accepted by the following element, the surplus air was discharged into dump regions which were vented to the environment by means of bleed holes. If the bleed holes of different elements were placed in close proximity to each other, it was found that these elements affected each other. To overcome this problem the elements were located either sufficiently far apart that bleed air from one element could not affect the performance of an adjacent element, or in such a position that their bleed air could not be trapped by adjacent bleed holes.

5.5 System Debugging

Figure 11 shows the logical design used in selecting and assembling the various fluidic elements. The location and function of each fluidic element are shown in Figure 12. By comparing Figures 11 and 12 it was possible to locate the exact function served by each element in the final model. In order to check the performance of a particular element during the operation of the model, it was necessary to connect manometers to all input and output tubes connected to that element. System debugging consisted either of tracing back a fault which appeared at the display panel, or of tracing forward the correct signals from the non-destructive memory, until the inconsistency was located.

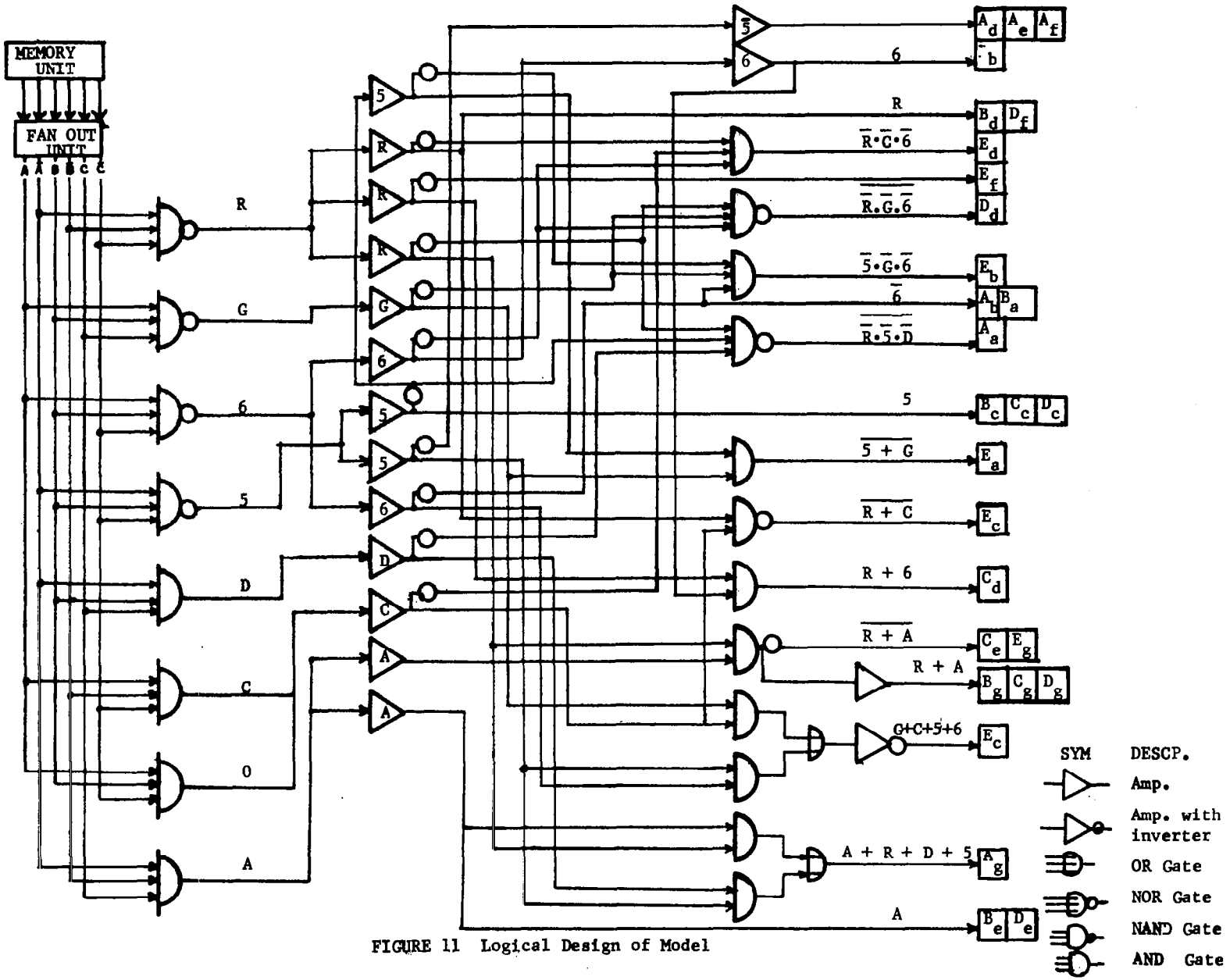

FIGURE 11 Logical Design of Model

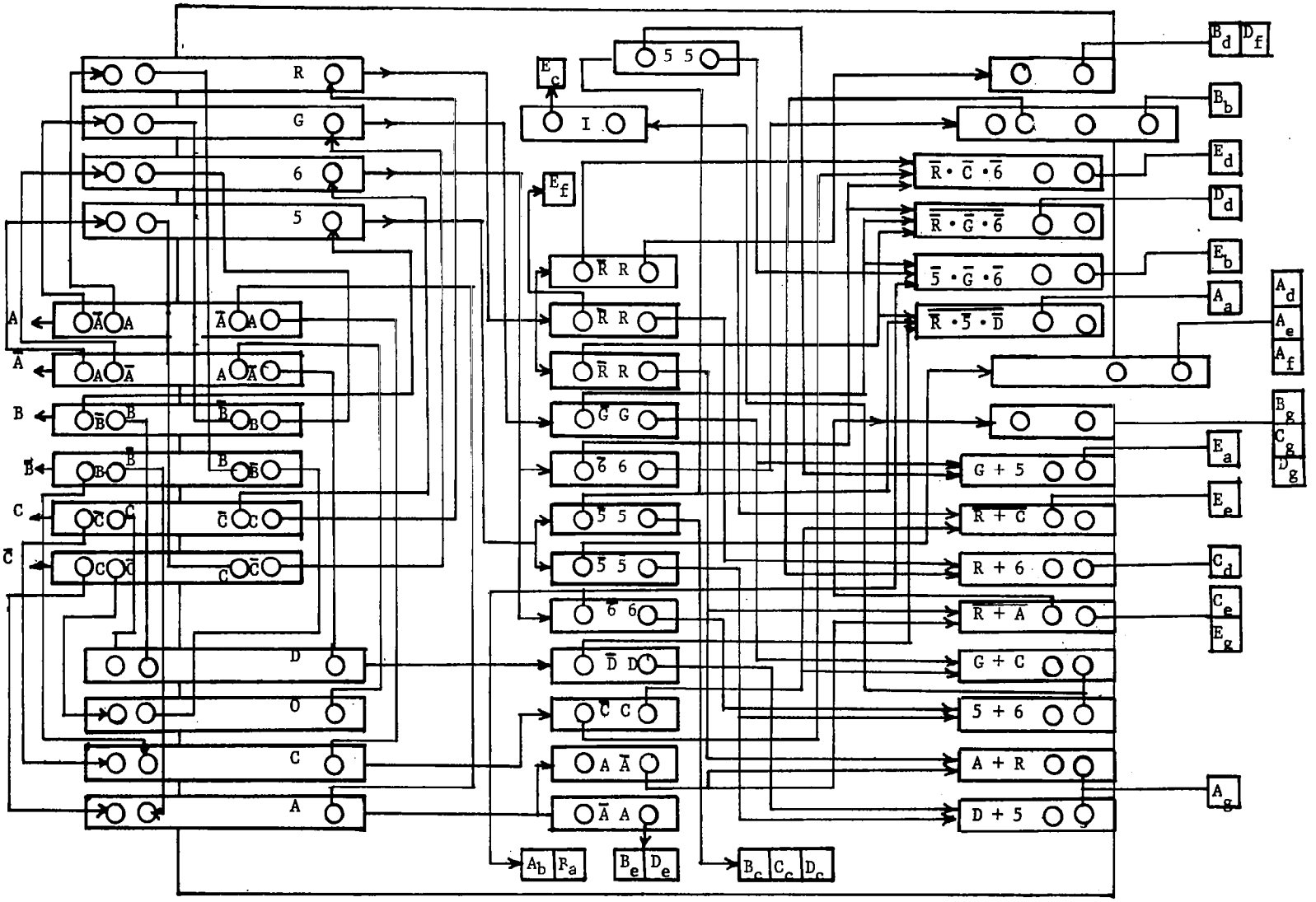

FIGURE 12 Schematic View of Elements As Viewed From Top of Model

VI. SUGGESTED AREAS FOR FUTURE STUDY

The non-destructive fluid memory opens up a new field in fluid logic systems. Since the information can be stored permanently inside the memory unit without the need for an auxilliary air supply, we have the basis for a fluidic removable memory, similar to a removable tape, which could be re-used indefinitely. Information may be loaded into a non-destructive fluidic memory by means of a tape or card. An independent unit designed specially to load or read out information may be used with transportable non-destructive memory modules. In this way data may be stored in library form ready for immediate use in a fluidic computer. Also, in digital control systems, the control path can be preprogrammed inside the memory unit in order to perform preselected tasks.

Beyond these applications, the combination of a non-destructive memory and a stable flip-flop permits various circuit applications, such as a synchronized flip-flop, a comparator device, a stable oscillator, a pulse multiplier, etc. Each example is illustrated in Figure 13, (a), (b), (c), (d). The non-destructive memory device and its associated logic can replace existing electronic circuits to form accumulators, shift registers, read and write devices, etc.

In the program to develop a non-destructive fluidic memory, no attempt was made to miniaturize any of the components. However, we feel that techniques can be developed which will enable us to achieve packaging densities of up to 10,000 elements per cubic inch. This estimate is based on the fact that, using relatively crude fabrication techniques, we have built a workable fluidic component measuring .1 x .1 x .01 inches.

We feel that non-destructive fluidic storage devices will also lend themselves to micro-miniaturization, and that "sheets" of these devices containing up to 100 per square inch can be developed to take the place of cards or punched paper tape. This form of information storage device will be superior, in that it will be reusable; it will also permit selective modification to the data it contains.

a. Synchronized Flip-Flop

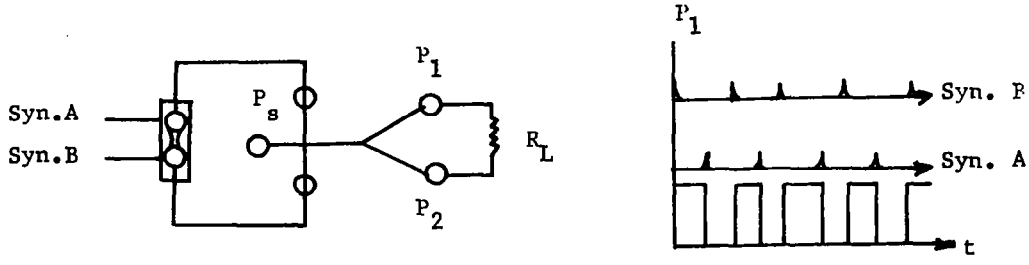

b. "Comparator" or "Polarity Indicator"

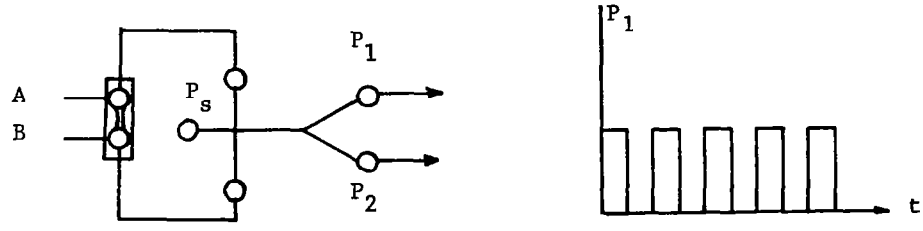

c. Stable Oscillator

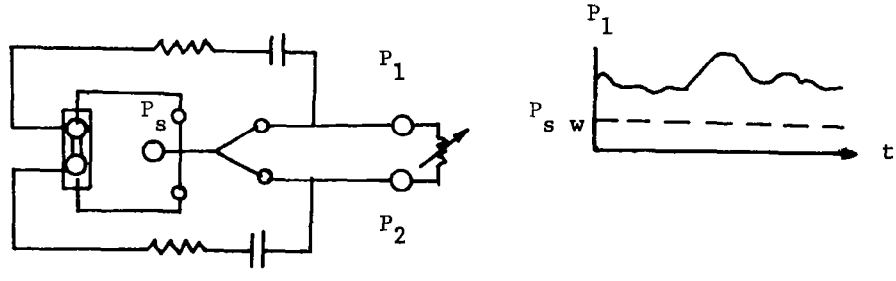

d. Pulse Multiplier

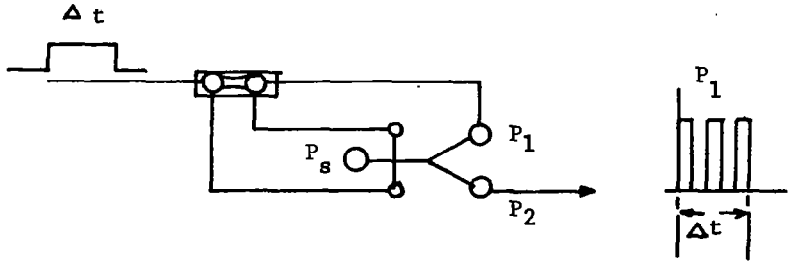

FIGURE 13

VII. CONCLUSION

The non-destructive fluidic memory has been shown to be a feasible concept. Tests on the demonstration model built for this contract have shown that data may be written fluidically into the memory using an IBM punched card, and may be read from the memory using conventional fluidic devices. A fluidic display, using elastomer beads, has been developed. The purpose of this display was to show that a readable fluidic output was feasible, and that the digital logic required to transform the information from the non-destructive memory elements into a recognizable display pattern could be developed.

No attempt was made during this phase of the program to design ultra-miniature devices having a high maximum switching rate, and it is to be expected that these memory elements will be slower than conventional fluidic devices using a gas only; however, speeds of the order of several hundred cycles per second may be anticipated. The application of a non-destructive storage device to high speed systems requiring only a short memory storage interval is therefore less useful than one in which mass storage of information is required for an extended period of time, such as on a deep space mission.

These investigations have successfully demonstrated that a new fluidic technology is possible. This technology has been called "two-phase fluidics" because fluids in both gaseous and liquid phases are used. The advantages of this new technology include: 1) the non-destructive memory feature, which was the subject of this report, 2) the infinite input impedance analog amplifier feature, which is the subject of current investigations being performed as an extension of the original non-destructive memory contract, and 3) an electric-to-fluid interface using the electro-capillarity effect. These features fulfill three of the most pressing needs felt by designers of fluidic systems.

Appendix A

MEMORY ELEMENT DESIGN CALCULATIONS

A.1 Analysis of Memory Element Switching Pressures*

A factor of prime importance to the design of the memory element is signal pressure expressed as a function of the radius of the restriction through which the bead must pass, the radius of the bead cavity, and the surface tension.

As the bead is forced through the restriction, it goes through various configurations as shown in Figures A-1 (a), (b), and (c).

Consider the memory fluid bead in the left cell. When P_{sw}, the switching pressure, is applied, the bead will be partially forced into the restriction as shown in Figure A-1(b).

The pressures in the menisci are:

$$(P - P_{sw}) = \frac{2\eta}{R} \cos \alpha_1 \qquad (1)$$

$$(P - P_a) = \frac{2\eta}{r} \cos \alpha_2 \qquad (2)$$

in which
- P = bead internal pressure
- P_{sw} = switching pressure
- α = angle between direction of surface forces and axis of chamber
- η = surface tension
- P_a = pressure in right cell
- R,r = radius of memory cell and switching path, respectively.

Note that the angles α_1 and α_2, which the surface forces form with the chamber axis and switching path walls, are numerically the same as the contact angle Φ_c of the bead on the wall. Equations (1) and (2) can be rearranged into:

$$\frac{2\eta}{R} \cos \alpha_1 + P_{sw} = \frac{2\eta}{r} \cos \alpha_2 + P_a \qquad (3)$$

Therefore, the differential pressure required to force the bead into the switching path is:

$$P_{sw} - P_a = \frac{2\eta}{r} \cos \alpha_2 - \frac{2\eta}{R} \cos \alpha_1 \qquad (4)$$

*by E. Martinez, Chief, Fluidic Systems, Giannini Controls Corporation, Astromechanics Research Division.

However, the information of interest here is the minimum differential switching pressure. This will be derived by considering the behavior of the right-hand meniscus at the time its line of contact goes past the corner of the restriction. (See Figure A-1 (c))

To clarify this point, let us now consider a sketch showing a magnified view of that corner, as in Figure A-2.

Since the contact angle is a function of the materials involved, it remains constant; i.e., the angle which the surface tension force makes with the solid surface is always the same. However, in the above geometry, the wall in contact with the mercury goes through a relatively abrupt 90° change. This has been shown for illustration in terms of a somewhat rounded corner. Therefore, as the wall angle sweeps through 90 degrees, the orientation of the surface forces with respect to the axis of the chamber will sweep likewise. It can then be seen that at some intermediate position of the meniscus, the surface forces will be exactly parallel to the axis of the chamber, i.e. the angle α_2 is equal to zero (although Φ_c remains the same).

At this point, the minimum differential switching pressure will be required. We may write Equation (4) for α_2 equal to zero on the right-hand meniscus and substitute the contact angle of the liquid Φ_c for α_1. (Note that it has been assumed that the bead volume is such that the left-hand meniscus has not changed diameter). We then obtain:

$$\left|P_{sw} - P_a\right|_{min.} = \frac{2\eta}{R}\left(\frac{R}{r} - \cos \Phi_c\right) \qquad (5)$$

For typical values, such as: R = .05 in., r = .025, $\Phi_c = 40^{\circ}$ and η = 0.00264 lbs./in. for mercury, the pressure differential for this case would be 3.6" H_2O.

This calculation does not take into account the friction of the bead in the chamber. Repeated measurements have shown that the bead-wall interface exhibits friction resulting in a pressure of the order of 0.70 inches of water for mercury and smooth plexiglass walls.

A series of experiments were conducted to obtain minimum required differential switching pressures for various R/r ratios. The results of these experiments are shown in Figure A-3. Equation (5) is also

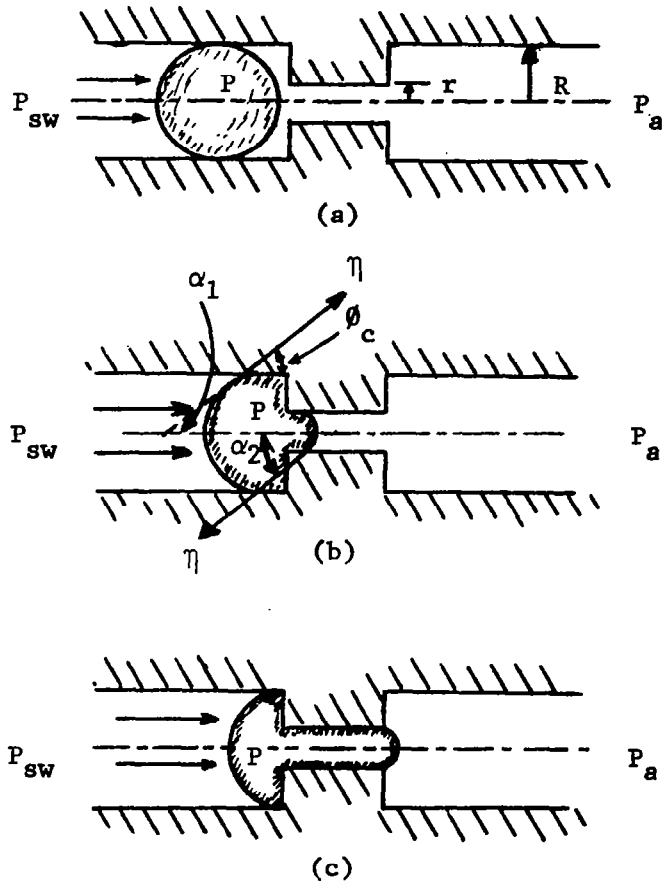

FIGURE A-1 Fluid Bead in Cell

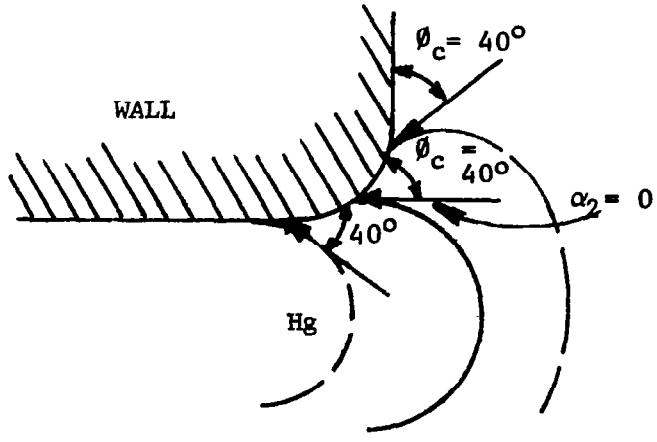

FIGURE A-2 Detail of Corner Showing Bead Progression

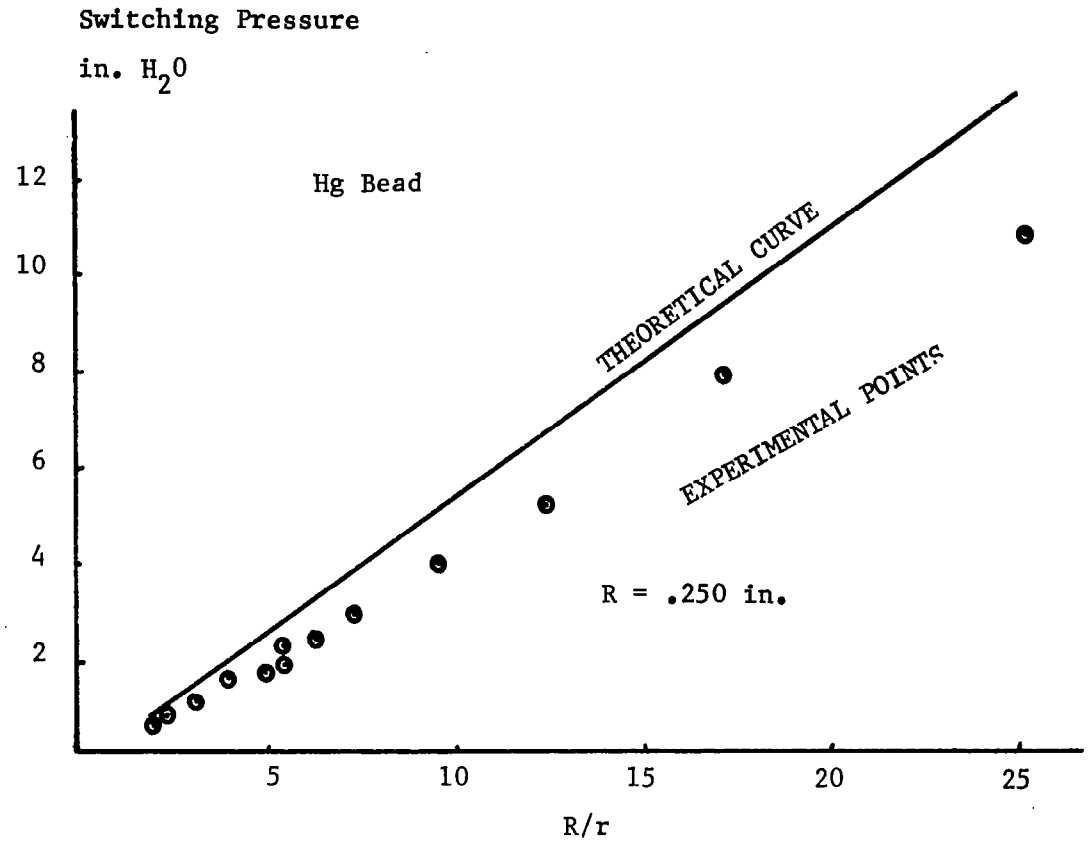

FIGURE A-3 Comparison of Experimental and Theoretical Results of the Minimum Differential Switching Pressure of a Memory Cell.

plotted in that Figure. The experimental curve exhibits excellent linearity; however its slope is about 23% less than the theoretical prediction. An examination of the form of equation (5), in addition to microscopic observation of the bead suggests that the probable cause of this discrepancy is an effective lowering of the surface tension due to impurities in the mercury.

A.2 Design Analysis of Memory Cell Geometry*

A primary requirement for the proper operation of the memory unit is the preservation of bead integrity. This is especially true for glycerine-silica beads. When a small drop of glycerine is coated with colloidal silica it exhibits high surface tension characteristics similar to those of mercury. However the glycerine bead cannot regroup itself after it breaks.

Although there are other forces acting on the bead, inertial forces appear to be the main mechanism causing break-up at the higher switching rates. These inertia forces are the result of the changes in the cross-section of the switching path. Therefore in order to minimize these effects and to extend the switching life of the bead, the cell geometry has to be carefully designed.

A complete analysis of the bead dynamic behavior is a difficult task. A number of assumptions will be made to make the problem more tractable. The problem will be defined first in a more general form using basic techniques of the calculus of variations. Later another constraint will be considered to satisfy the problem further and to obtain a useful, if not complete, expression for the switching path geometry. Let us consider a cell configuration such as the one shown in Figure A-4(a). It consists of two chambers connected through a narrow channel of varying cross-section. For the purpose of this analysis the following assumptions will be made: 1) gravity forces are negligible compared to the other forces acting on the bead; 2) the bead moves without friction; 3) the effects of the surface tension on the menisci are only considered insofar as they cause the bead to fill the space between the walls and in effect attach to

*By E. Martinez, Chief, Fluidic Systems.

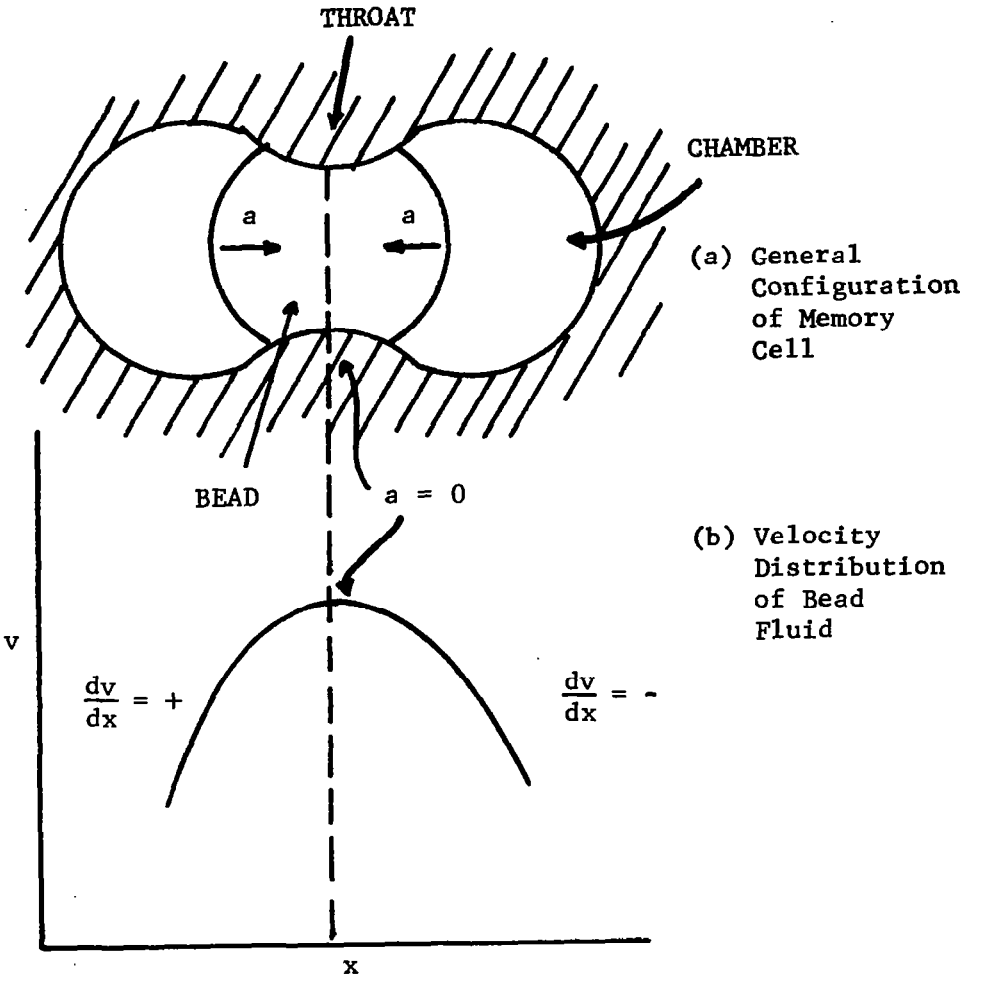
THROAT
CHAMBER
a
a
(a) General Configuration of Memory Cell
BEAD
a = 0
(b) Velocity Distribution of Bead Fluid
v
dv/dx = +
dv/dx = -
x

FIGURE A-4

the walls; 4) the menisci will be approximated by flat surfaces; and 5) the bead fluid is incompressible. The switching path is of circular cross-section and has fore-aft symmetry.

As the bead moves from left to right through the restriction the portion of the bead to the left of the throat (minimum area section) is under acceleration. Due to the decreasing area of the path, the portion of the bead to the right of the throat will be decelerating where the path area is increasing. The velocity at the various sections of the bead are represented in Figure A-4(b).

The regions of the bead fluid to the right of the throat are undergoing deceleration; therefore a force must be acting on the fluid to slow it down. This force is the surface tension acting on the circumference of the section. The point of maximum stress is at the throat. The surface tension force there must provide the decelerating force for all the fluid in the right-hand region of the bead. If the surface tension force that can be produced at the throat is lower than the inertia force generated by the rate of enlargement of the switching channel, the bead will break at that point and a separate drop or bead will detach itself from the original bead mass.

In order to compute these forces and to find the optimum cell geometry, let us consider an elemental section in the right region of the bead. The acceleration force acting on this section is (see Figure A-5)

$$dF = a(x)dm(x) \tag{6}$$

The acceleration may be written:

$$a = \frac{dv}{dt} = \frac{dv}{dr} \cdot \frac{dr}{dx} \cdot \frac{dx}{dt} \tag{7}$$

Since the fluid is incompressible the velocity at any section is:

$$v = \frac{Q}{\pi r^2} \tag{8}$$

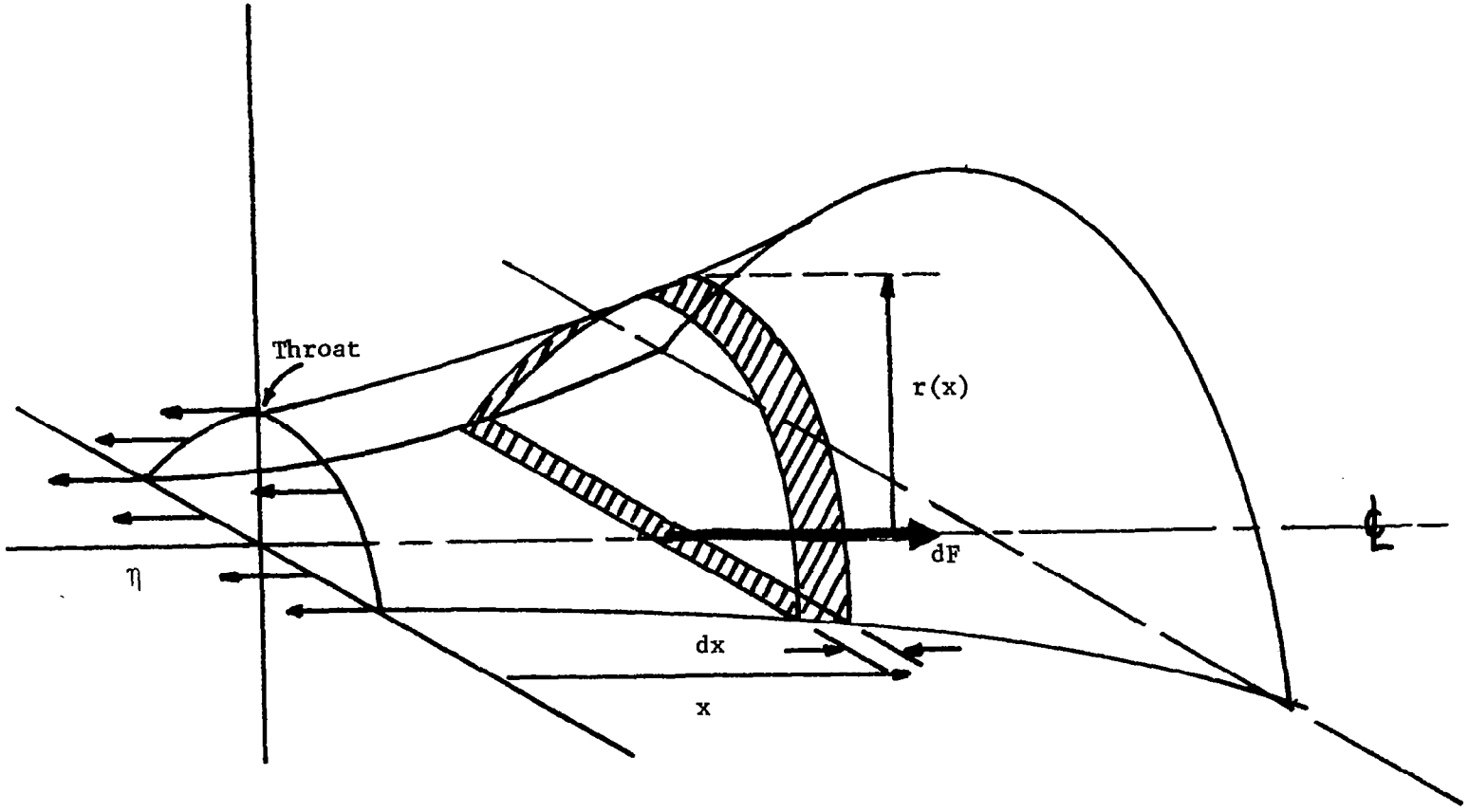

FIGURE A-5 Bead Force Balance

Then $$\frac{dv}{dr} = \frac{-2Q}{\pi r^3} \tag{9}$$

and

$$\frac{dx}{dt} = v = \frac{Q}{\pi r^2} \tag{10}$$

$$dm = \rho \pi r^2 dx \tag{11}$$

Therefore:

$$dF = \frac{-2\rho Q^2}{\pi r^3} \left(\frac{dr}{dx}\right) \quad dx \tag{12}$$

To find the total force, integrating with the following boundary conditions:

$$\text{at } x = 0 \qquad r = r_t \qquad F = F_t$$

$$\text{at } x = x \qquad r = r \qquad F = 0 \tag{13}$$

we have

$$\int_{F_t}^{0} dF = \frac{-2\rho Q^2}{\pi} \int_0^x \frac{1}{r^3} \frac{dr}{dx} dx \tag{14}$$

or

$$F_t = \frac{2\rho Q^2}{\pi} \int_0^x \frac{1}{r^3} \frac{dr}{dx} dx \tag{15}$$

The force F_t is the total force at the throat tending to pull the bead apart. To maintain integrity the surface tension must be equal or larger than that force. i.e.:

$$2\pi r_t \eta \geq F_t \tag{16}$$

Clearly it is desirable to minimize F_t, which is a function of the switching path configuration. The problem reduces, then, to the computation of a non-trivial extremum of the functional, f*:

$$f^* = \frac{2\rho Q^2}{\pi}\left(\frac{1}{r^3}\frac{dr}{dx}\right) \tag{17}$$

between $x = 0$ and $x = x$. If it has an extremum, this functional must satisfy the Euler equation:

$$\frac{\partial f^*}{\partial r} - \frac{d}{dx}\frac{\partial f^*}{\partial \dot{r}} = 0 \tag{18}$$

where in this notation $\dot{r} = dr/dx$. Carrying out the operations using the functional (17) we obtain:

$$\frac{\partial f^*}{\partial r} = \frac{-6\rho Q^2}{\pi}\frac{\dot{r}}{r^4} \tag{19}$$

$$\frac{d}{dx}\frac{\partial f^*}{\partial \dot{r}} = \frac{-6\rho Q^2}{\pi}\frac{\dot{r}}{r^4}$$

It can be seen that Euler's equation is identically satisfied. Therefore the geometry of the contour does not affect the total force generated between the throat and a given fixed point to the right of the throat. The force is a function only of the end points. However, this solution does not preclude the possibility of localized high decelerations with the corresponding high stresses generated at the surface of the bead. To account for this an additional constraint is necessary. The most logical constraint in this case is to postulate a constant acceleration profile, i.e. a profile that produces an equal acceleration at any of the sections of the bead.

The expression for the acceleration at an arbitrary cross-section may be obtained using equation(7):

$$a = \frac{dv}{dt} = -\frac{2Q^2}{\pi^2 r^5}\frac{dr}{dx} \tag{20}$$

Then:

$$\frac{1}{r^5}\frac{dr}{dx} = \frac{-a\pi^2}{2Q^2} \tag{20A}$$

We will limit that acceleration to the level which will produce a force at the throat equal to the surface tension force at that section. Thus:

$$a = \frac{-F}{m} = - \frac{2\pi r_t \eta}{m} \tag{21}$$

and

$$\frac{dr}{r^5} = \frac{\pi^3 r_t \eta}{mQ^2} dx \tag{22}$$

Using boundary condition 13 we integrate (22):

$$\int_{r_t}^{r} \frac{dr}{r^5} = \frac{\pi^3 r_t \eta}{mQ^2} \int_0^x dx \tag{23}$$

or:

$$\frac{\pi^3 r_t \eta}{mQ^2} x = - \frac{1}{4} \left(\frac{1}{r^4} - \frac{1}{r_t^4} \right) \tag{24}$$

Solving for r:

$$r = \sqrt[4]{\frac{1}{A - Bx}} \tag{25}$$

where

$$A = \frac{1}{r_t^4}$$

$$B = \frac{4\pi^3 r_t \eta}{mQ^2}$$

For a given bead fluid and switching speed (25) represents the limiting contour (at which bead failure will occur), producing constant acceleration (negative) throughout the right region of the bead. Similar curves within this contour will provide a margin of safety.

Another approach is to consider the balance between the kinetic energy introduced into the right side of the bead and the potential energy or work done by the surface tension.

At the time when the whole bead has just passed the throat, the net change in kinetic energy is:

$$\Delta(KE) = (KE)_{in.} - (KE)_{remains} \tag{26}$$

Written in terms of the cell parameters:

$$\Delta(KE) = \frac{\rho V Q^2}{2\pi^2}\left(\frac{1}{r_t^4} - \frac{1}{r^4}\right) \tag{27}$$

The work done by the surface tension is

$\Delta PE = \eta \cdot$ change in surface area to the right of throat

$$\Delta(PE) = 2\pi\eta \int_0^x r\sqrt{1 + \left(\frac{dr}{dx}\right)^2}\, dx + \pi\eta(r^2 - r_t^2) \tag{28}$$

In order to simplify the problem the change in potential energy of the meniscus is neglected.

Under these circumstances the problem reduces to the search for contour that produces a certain change in potential energy for the minimum area change. Or in other words the countour that minimizes the integral:

$$\int_0^x r\sqrt{1 + \dot{r}^2}\, dx \tag{29}$$

The functional then must satisfy Euler's equation as before. Thus:

$$1 - \dot{r}^2 - \frac{r\ddot{r}}{1 + \dot{r}^2} = 0 \tag{30}$$

Using the conditions that $r = r_t$, $\dot{r} = 0$, this differential equation has the first integral:

$$r\sqrt{1+\dot{r}^2} - \frac{r\dot{r}^2}{\sqrt{1+\dot{r}^2}} = r_t \tag{31}$$

that can be separated to obtain:

$$\int_0^x dx = r_t \int_{r_t}^{r} \frac{dr}{\sqrt{r^2 - r_t^2}} \tag{32}$$

Carrying out the integration and rearranging the results, we have:

$$\frac{r}{r_t} = \cosh \frac{x}{r_t} \tag{33}$$

This equation is plotted in Figure A-6(b). This contour exhibits the minimum surface for a given potential energy change. This can be interpreted approximately as a constant force contour, i.e. the force at any section is constant.

An example will now be considered using the results of the first analysis.

EXAMPLE

The limiting constant acceleration contour is required for a mercury unit with the following characteristics:

Switching path throat: $r_t = .010$ in.

Mercury bead, $\eta = .00264$ lb./in. and $\rho = 1.52 \cdot 10^{-2}$ slugs/in.^{3}

Bead mass, $m = 1.24 \cdot 10^{-7}$ slugs (radius of sphere 0.0125 in.)

Required switching frequency: 100 switchings per second.

$$Q = 100 \quad V = 100 \frac{m}{\rho} = 8.18 \cdot 10^{-4} \frac{\text{in.}^3}{\text{sec.}} \tag{34}$$

Then from equation (25): $$r = \sqrt[4]{\frac{1}{10^8 - 4.74 \cdot 10^{11} x}} \tag{35}$$

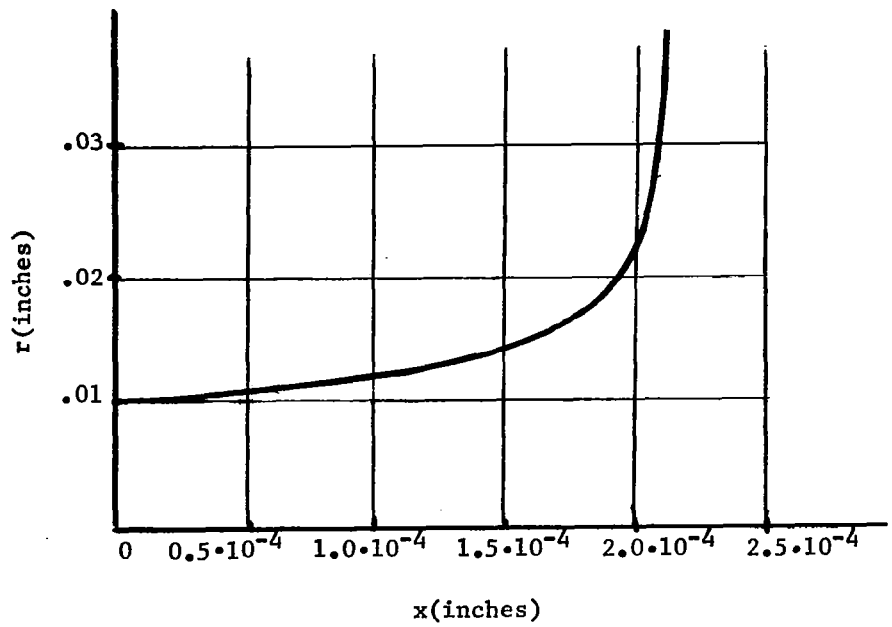

FIGURE A-6(a) Limiting constant-acceleration contour

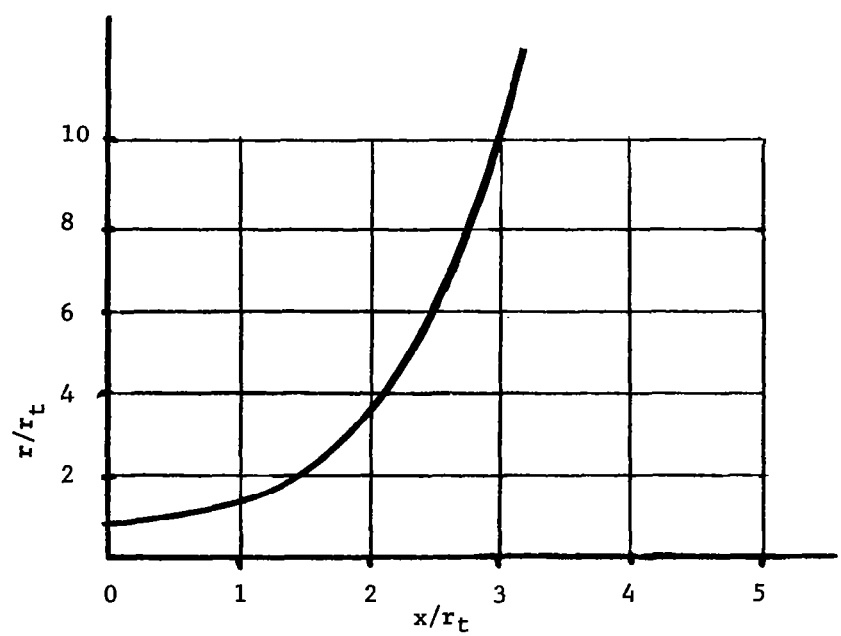

FIGURE A-6(b) Limiting contour for minimum bead surface deformation (constant-force approximation)

This is plotted in Figure A-6(a). It can be seen from this figure that the limiting constant acceleration contour is quite abrupt; i.e. the transition from the throat to the chambers can be accomplished in a very short length.

A.3 Analysis of Low Level Sensing Circuit

Since the glycerine bead has a surface tension of about half that of mercury, the required switching pressure, P_{sw}, is correspondingly low. For example, a .07" diameter bead needs only .3 to .5 inches of water switching pressure. The sensing pressure can not be larger than P_{sw}; therefore, to obtain a maximum sensing pressure difference between the "1" and "0" states, analysis of the sensing circuit is necessary. Assuming the Reynolds number is low, pressure drop along an impedance is linear. An equivalent circuit of the memory cell may be drawn as shown in Figure A-7(a) and (b).

STATE "1"

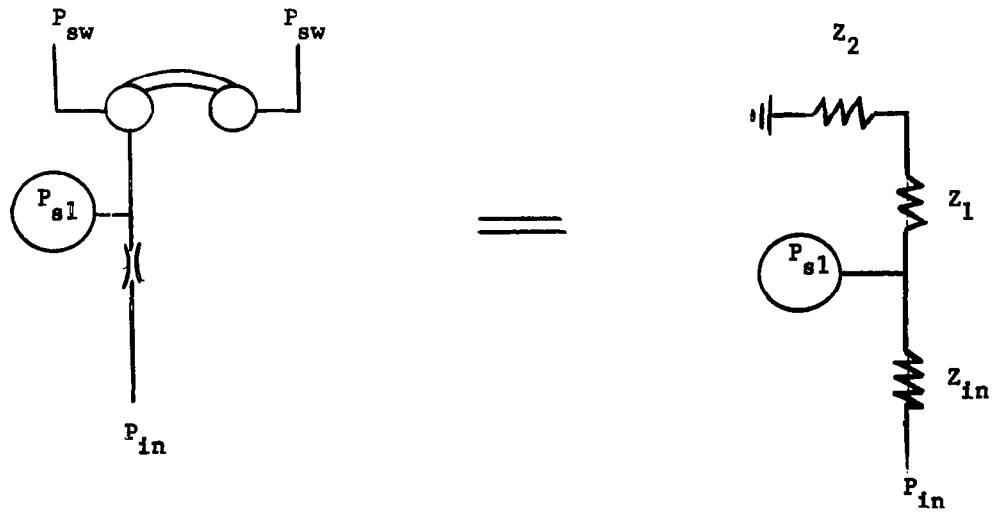

FIGURE A-7(a)

STATE "0"

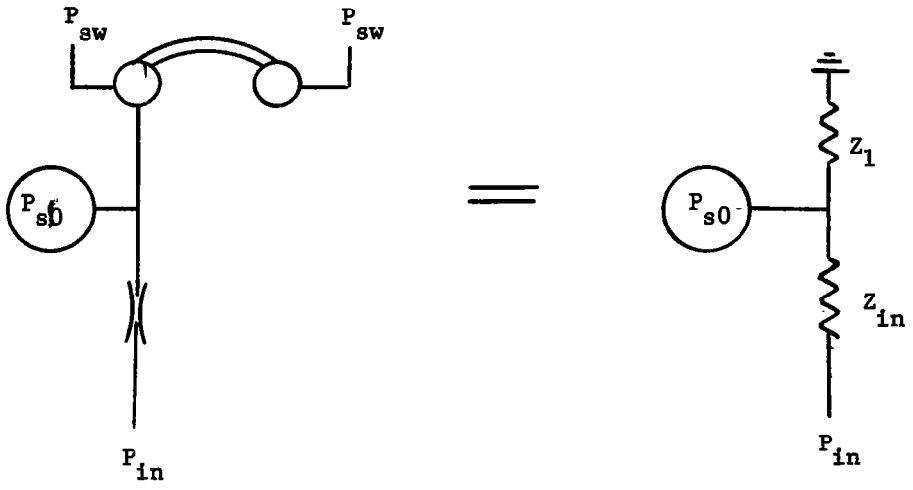

FIGURE A-7(b)

For simplicity in analyzing the circuit, assume the sensing device does not draw air flow. Let:

P_{s1}, P_{s0} = sensing pressures in "1" and "0" states
ΔP_{sn} = difference in sensing pressures
Z_1 = sensing hole impedance
Z_2 = leakage impedance
Z_{in} = input series impedance
P_{in} = sensing pressure supply

Therefore:

STATE "1" $$P_{s1} = \frac{P_{in}(Z_1 + Z_2)}{Z_1 + Z_2 + Z_{in}} \tag{35}$$

STATE "0" $$P_{s0} = \frac{P_{in}Z_1}{Z_1 + Z_{in}} \tag{36}$$

$$\Delta P_{sn} = P_{s1} - P_{s0} = P_{in}\left[\frac{Z_1 + Z_2}{Z_1 + Z_2 + Z_{in}} - \frac{Z_1}{Z_1 + Z_{in}}\right] \tag{37}$$

In practical cases in which Z_1, Z_2 can be found, it is desirable to find Z_{in} for a maximum ΔP_{sn}. Before we go further, let us check for two extreme conditions: when Z_{in} is equal to 0, and infinity.

CASE I $\quad Z_{in} = 0 \quad$ then $\Delta P_{sn} = 0$

CASE II $\quad Z_{in} = \infty \quad$ then $\Delta P_{sn} = 0$

when $\quad Z_{in} \neq 0 \neq \infty \quad$ then $\Delta P_{sn} \neq 0$

These will be discussed as follows:

Rewriting equation (37):

$$\Delta P_{sn} = \left[\frac{1}{1 + \frac{Z_{in}}{Z_1 + Z_2}} - \frac{1}{1 + \frac{Z_{in}}{Z_1}} \right] P_{in} \tag{38}$$

let $Z_{in}/Z_1 = h$, and $Z_1/Z_2 = k$; then equation (38) can be written:

$$\frac{\Delta P_{sn}}{P_{in}} = \left[\left(\frac{1}{1 + \frac{h}{1 + \frac{1}{k}}} \right) - \left(\frac{1}{1 + h} \right) \right] \tag{39}$$

Figure A-8 shows plots of $\Delta P_{sn}/P_{in}$ against h for different values of the ratio k. The maxima of each curve is found by differentiating equation (39) with respect to h or Z_{in}/Z_1:

$$\frac{\partial \left(\frac{\Delta P_{sn}}{P_{in}} \right)}{\partial h} = \frac{\partial}{\partial h} \left[\frac{1}{1 + \frac{h}{1 + \frac{1}{k}}} - \frac{1}{1 + h} \right]$$

$$\text{let } \delta = \frac{k}{1 + k}$$

$$\frac{\partial \left(\frac{\Delta P_{sn}}{P_{in}} \right)}{\partial h} = \frac{\partial}{\partial h} \left[\frac{1}{1 + \delta h} - \frac{1}{1 + h} \right]$$

$$\frac{\partial \left(\frac{\Delta P_{sn}}{P_{in}} \right)}{\partial h} = - \frac{\delta}{(1 + \delta h)^2} + \frac{1}{(1 + h)^2} \tag{40}$$

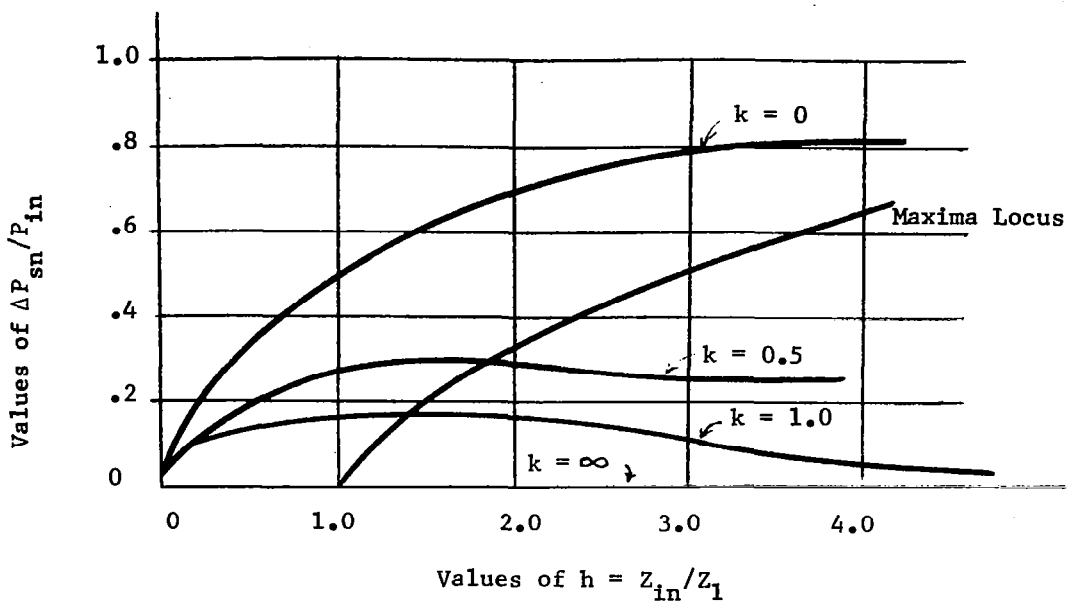

FIGURE A-8

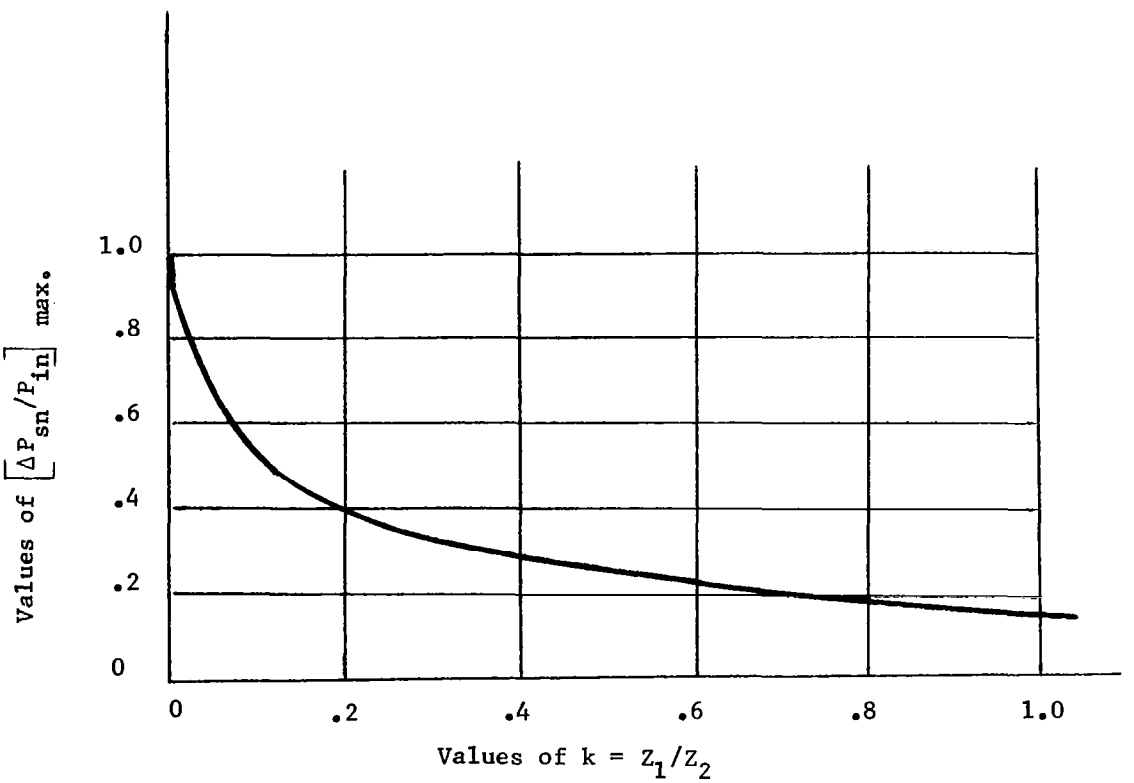

FIGURE A-9

Set equation (40) = 0,

$$\frac{\delta}{(1 + \delta h)^2} = \frac{1}{(1 + h)^2}$$

or

$$h = \frac{\sqrt{\delta} - 1}{\delta - \sqrt{\delta}} = \frac{1}{\sqrt{\delta}}$$

$$\frac{Z_{in}}{Z_1} = \sqrt{\frac{1 + k}{k}} \tag{41}$$

Equation (41) gives the locus of maxima at different values of k. For example: $k = 0$, $Z_{in}/Z_1 = \infty$, $k = 1.0$, $Z_{in}/Z_1 = 1.41$, etc. From Figure A-8, it can be seen that Z_{in} becomes less important when k approaches 0, and is more critical when k becomes large.

For a small sensing hole when Z_1 is large, or k ratio is large, (close to 1), a low Z_{in} is required. For a large sensing hole k is small and a high Z_{in} is required. But after a certain h ratio, Z_{in} has little effect on ΔP_{sn}. To find Z_{in} exactly for maximum ΔP_{sn}, we substitute $k = Z_1/Z_2$ into equation (41) and obtain:

$$\frac{Z_{in}}{Z_1} = \sqrt{\frac{1 + Z_1/Z_2}{Z_1/Z_2}}$$

$$Z_{in} = \sqrt{Z_1^2 + Z_1 Z_2} \tag{42}$$

Equation (42) gives Z_{in} values as related to Z_1 and Z_2. Going one step further, we put equation (42) into equation (38), thereby showing how k value affects $\left[\Delta P_{sn}/P_{in}\right]_{max.}$

$$\left[\frac{\Delta P_{sn}}{P_{in}}\right]_{max.} = \left[\frac{1}{1 + (\sqrt{Z_1(Z_1 + Z_2)})/(Z_1 + Z_2)} - \frac{1}{1 + \sqrt{Z_1(Z_1 + Z_2)}/Z_1}\right]$$

$$\left[\frac{\Delta P_{sn}}{P_{in}}\right]_{max.} = \frac{\sqrt{1 + k}}{\sqrt{1 + k} + \sqrt{k}} - \frac{1}{1 + \sqrt{1 + 1/k}} \tag{43}$$

Equation (43) is plotted in Figure A-9. It may be observed that when $k > .3$, the change of $\left[\Delta P_{sn}/P_{in}\right]_{max.}$ is decreasingly significant. Therefore the lower values of k have more effect on $\left[\Delta P_{sn}/P_{in}\right]_{max.}$.

A.4 Conclusions

By considering the above discussion concerning increasing ΔP_{sn}, it is found that the following methods can be used:

1) Increase the sensing pressure supply P_{in}.
2) Choose the Z_{in}/Z_1 ratio, for max. ΔP_{sn}
3) For the same Z_{in}/Z_1 ratio, increase Z_2, to obtain a better ΔP_{sn}.

1) Increasing P_{in} is an easy method, but P_{in} is limited since it cannot exceed switching pressure, P_{sw}. Otherwise P_{in} will cause the fluid bead to switch.

2) Z_2 can be increased by decreasing the air leakage around the bead. This occurrence can be achieved by using a small memory cell and a relatively large bead. A new problem arises here, however, for it is uncertain how much compression a bead can stand.

3) The choice of the Z_{in}/Z_1 ratio for maximum ΔP_{sn} is another way to increase ΔP_{sn}. Changing Z_{in} is an important method, resulting from circuit analysis.

In conclusion, in order to increase the ΔP_{sn} value, all the methods will be applied to obtain the maximum ΔP_{sn}. But there is another point that has not been made yet; that is, how can the sensing pressure ΔP_{sn} be utilized. To amplify ΔP_{sn}, an infinite-input-impedance amplifier is needed. Figure A-10 shows the circuit for a conventional pressure amplifier. (See next page.) The impedance Z_L is the input impedance of the amplifier. Therefore, equations (35) and (36) will be modified as:

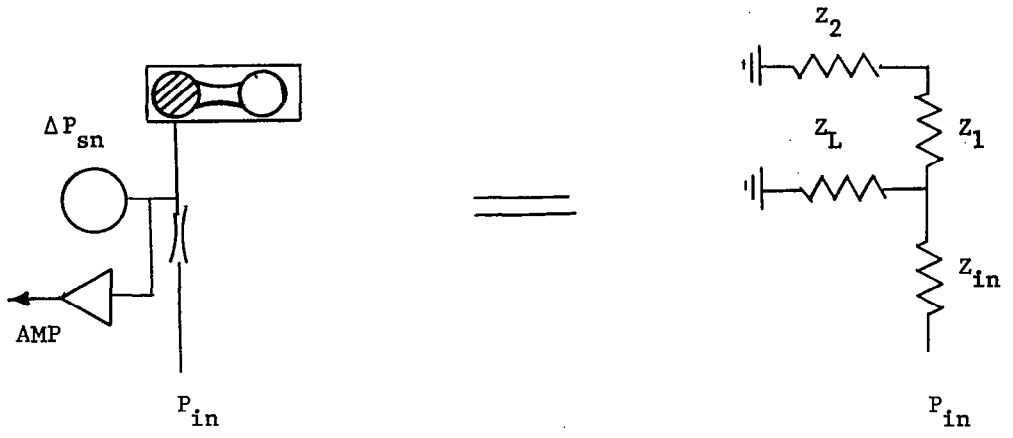

FIGURE A-10

STATE "1"

$$P_{s1} = P_{in} \frac{\frac{(Z_1 + Z_2)Z_L}{Z_1 + Z_2 + Z_L}}{Z_{in} + \frac{(Z_1 + Z_2)Z_L}{Z_1 + Z_2 + Z_L}} \tag{44}$$

STATE "0"

$$P_{s0} = P_{in} \frac{\frac{Z_1 Z_L}{Z_1 + Z_L}}{Z_{in} + \frac{Z_1 Z_L}{Z_1 + Z_L}} \tag{45}$$

And,

$$\Delta P_{sn} = P_{s1} - P_{s0} = P_{in} \left[\frac{Z_a}{Z_{in} + Z_a} - \frac{Z_b}{Z_{in} + Z_b} \right] \tag{46}$$

in which

$$Z_a + \frac{(Z_1 + Z_2)Z_L}{Z_1 + Z_2 + Z_L} = \frac{Z_1 + Z_2}{(Z_1 + Z_2)/Z_L + 1}$$

$$Z_b = \frac{Z_1 Z_L}{Z_1 + Z_L} = \frac{Z_1}{Z_1/Z_L + 1} \tag{47}$$

If $Z_L \ll Z_1$, then $Z_a = Z_b \cong Z_L$ and $\Delta P_{sn} = 0$.

This result shows that the value of the input impedance of a sensing amplifier is a very important factor in the sensing circuit. Therefore a very high input impedance is necessary to amplify the sensing signal.

Appendix B

MEMORY FLUID STUDY

by

Dr. L. L. Pytlewski

B.1 The Coated Bead Concept

This investigation was based upon a need for a substitute for the mercury beads originally proposed as switching elements for the fluidic memory device. Although mercury functions extremely well in these devices, conditions can arise whereby the toxic and corrosive properties of the liquid metal can become detrimental to a mission.

Knowledge of the chemical and physical properties of surfaces (solid and liquid) and chemical reactions occurring at surfaces supported a strong belief that the useful properties of mercury could be duplicated using materials which are non-toxic. Of the several pathways available, it was thought that a direct substitution of mercury with some kind of flexible bead in the "going" fluidic devices would produce more information, more rapidly.

No single liquid could be found which would not wet the surface of the methacrylate plastic cavities (trade names, Plexiglass, Lucite). However, the wetting (spreading) characteristics of most common surfaces can be radically changed (reversed) by the use of chemical surface-active agents. Most useful surfaces carry a negative charge. There are a large number of chemical compounds available, which, in solution, carry a positive charge (through dissociation); and absorb into these surfaces quite strongly. There are a number of cationic (as they are called) surfactants which contain at least one long-chain organic group or a perfluorinated organic group. Two examples are cited below:

a.

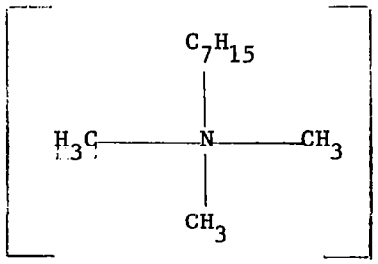

Component (or ion) which absorbs on negatively charged surfaces such as glass, plexiglass, paper, textiles.

Trimethyl heptyl ammonium chloride

b.

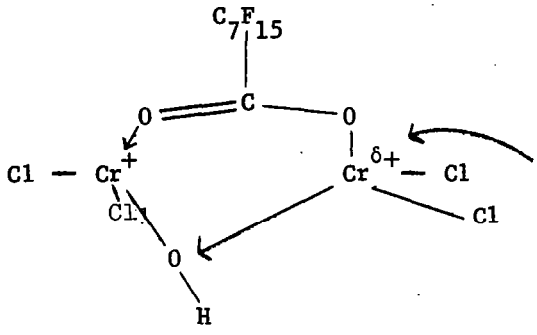

"Scotchgard" (FC805; 3M Company)

A perfluorooctanoic acid complex of $Cr(OH)Cl_2$.

Source of positive charge for surface attachment.

Both of these compounds, and many like these, will modify the substrate characteristics only because they form monomolecular layers (or very thin films in the case of polymers). Therefore, hydrophilic surfaces (as are all negative surfaces) become hydrophobic when treated and the treatments are substantive. Indeed! The perfluoroinated cationic surfactants produce surfaces which are not only hydrophobic, but also organo (organic liquid repellent or oleo) phobic, and dry powder repellant.

Fluidic plexiglass devices have had their surface characteristics modified using two fluorochemical surfactants; FC805 by 3M company and Zepel by duPont. The "Zepel" treatment has been shown to be far more effective with regard to the total properties of fluidic devices. The "Zepel" treatment is easy to apply (comes as a spray) and is quite resistant to removal by ordinary methods of cleaning. In fact, the net effect is to equate all substrates using the Zepel treatment. There are many single liquids which "roll" on the "Zepel" treated methacrylate surface. Just to name a few H_2O, glycerine, benzene, paraffin oil, Nujol.

The interaction of a liquid bead with a Zepel treated surface is greatly enhanced when a single liquid is coated with a fine adherent powder to form a two layer sphere. The fine powders must be chemically inert and adhere in a uniform layer to the liquid surface. An additional advantage with regard to the powder surface is the reduction of the volatility of the liquid.

It was found that the most useful powders are in the colloidal particle size range (10^{-4} - 10^{-5} cm diameter) and there are several of these commercially available.

Many spheres of all size ranges have been successfully generated

using glycerine, triethanolamine, and water as liquids and graphite, glass, silicas, diatomaceous earths, titania, and gold as powder coverings. In fact, a large number of combinations are possible and have been shown to be successful as stable switching beads in "Zepel" treated plexiglass memory units.

Of all of the aforementioned combinations of liquid-powder beads, the best appears to be composed of the following:

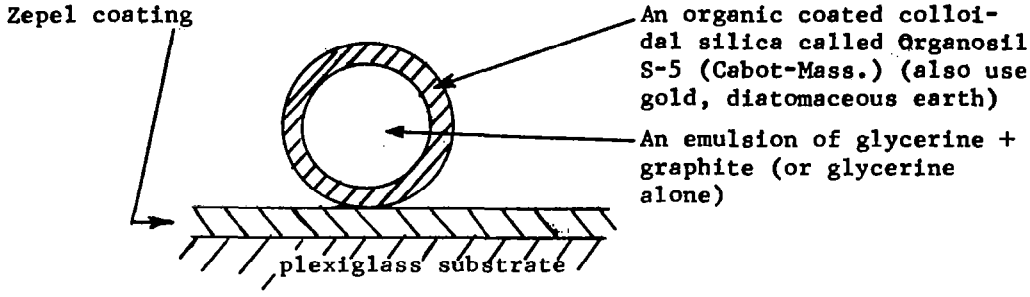

The beads formed are exceptionally stable with regard to constriction through switching orifices. High switching oscillation rates have been used without sign of breakup. In fact, these beads are more resistant to breaking than those of mercury. Switching has been demonstrated with beads that almost entirely fill up the chambers of a fluidic memory device.

B.2 Composition Studies of Bead Structure

The use of composite beads has resulted in vast improvements in performance over those single fluids tested so far. Mechanical changes in the structure of the solid substrate memory devices have been carried out and these show great promise as memory beads.

Earlier observations with regard to the operation of the glycerine and silica coated bead have strongly suggested that two substrate characteristics are required for most effective operations. These are:

a) The substrate surface must be smooth (mirror-like if possible),

b) a multiple coat of the fluorocarbon (Zepel-duPont) increases effectiveness.

The glycerine-silica coated bead composite has been improved as follows:
a) Glycerine freezes at 0° C (with difficulty). The addition of water to glycerine produces a lowering of the freezing point of the solution, a temperature of -40° C (-40°F) with a mixture of 1 volume of glycerine to

1 volume of water. Additionally, glycerine and water mixtures produce a "continuous" azeotrope so that evaporation of water (or absorption of water) should not occur readily thus producing very stable solutions.
b) It was found that transition metal salts in general are very soluble in the 1:1 glycerine and water solutions. In fact, the solubilities of some of these salts are high enough to make this a chemical problem worth investigating in itself. The effect of the solubility of the metal salts is to increase the surface tension of the solution of glycerine and water. With the increased surface tension we have an increase in the tendency of the bead to form a sphere. Furthermore, the presence of the salt in the glycerine-water systems produces a medium of high electrical conductivity.
c) The addition of water to glycerine improves the contact angle of the bead with the fluorocarbon surface. The contact angle of water alone on fluorocarbon-treated surfaces is the largest of all known single liquids.

B.3 Bead Preparation

The composite bead is produced in the following manner:

1. Equal volumes of glycerine and water are mixed well.
2. A transition metal salt (avoid the nitrates for the sake of safety) is added to the aqueous glycerine with stirring.

The investigator found that anhydrous Iron III chloride rapidly produces a very stable viscous solution.

Since the solution is exothermic, it is advised that the operation of solution be carried out in a container cooled with tap water at room temperature. It has been found that a forty cc. volume of the glycerine water solution will dissolve up to 150 - 200 gms. of anhydrous $FeCl_3$. It is suggested that effective ternary solutions are produced with approximately 100 gms. of $FeCl_3$ in 40 cc. of aqueous glycerine (1:1 by volume).

To form a bead, take a spoonful of organosil S-5 (by Cabot Corp. - Boston, Mass.) and spread into a smooth layer, about 1/8" deep, on a paper surface. A droplet of the above solution of the desired size is placed onto the organosil powder and then rolled about to achieve an overall smooth coating. The bead is then rolled free of the layer of powder and allowed to roll on a clean paper surface to remove any excess and agglomerates. The bead is then added to the device under

study by rolling along a channel in the paper and allowed to drop in place, carefully.

B.4 Summary

The chemical investigation carried out on bead systems has produced the following facts:

a) The glycerine-water solution is, by far, the best liquid for bead formation.

b) The organosil S - 5 powder is still the best bead surface coating.

c) The Zepel - duPont substrate treatment remains the best known surface treatment.

d) The addition of a transition metal salt as a surface tension enhancer and an electrical conductor are now the best known substances for bead self-consistency (hold-togetherness).

B.5 Conclusion

A memory device has been made using a fluorocarbon-treated cavity and non-mercury beads. The beads are non-toxic. The liquids used have vapor pressures below that of mercury through the normal physiological range of temperatures. The powder + liquid beads apparently can do everything that mercury can do in the single memory elements. In addition, electrical conduction is possible using the graphite-glycerine and gold-glycerine and glycerine-water-transition metal salt beads.

B.6 Prospects

It is strongly recommended that a series of transition metal salts + glycerine and water mixtures be tested for switching stability and longevity. In addition, some preliminary tests carried out by the author indicate that the new composite bead will be equally effective in analog system switching. It is strongly recommended that parallel efforts be made with digital and analog components.

B.7 Sources of Materials

1) Zepel-Water and Stain repeller in spray can. Available as experimental sample only from:

E. I. duPont de Nemours
Marshall Research Laboratory
Dr. Orville H. Bullitt, Director
3500 Grays Ferry Avenue
Philadelphia, Pennsylvania

2) Organo-Sil S-5, a colloidal silica.

Cabot Corporation
Oxides Division
125 High Street
Boston, Massachusetts 02110

3) Distilled or deionized water.

4) Anhydrous $FeCl_3$, Reagent grade, Sublimed

Supplier:
Matheson Coleman and Bell
East Rutherford, New Jersey
Catalogue number: FX215

5) Glycerine (Glycerol) Reagent grade

Any chemical supply house.

Appendix C

SWITCHING PERFORMANCE OF THE GLYCERINE BASE BEAD

C.1 Life Test of the Glycerine Base Bead

Switching tests showed that by multiple applications of Zepel to the walls of the bead container, the life of almost all beads tested may be extended indefinitely. For example, a .065" diameter glycerine bead with gold dust in suspension, coated with organic silica has shown no sign of deterioration after 250,000 switching cycles. This corresponds to 500,000 actual switching operations. The same type of bead was subjected to a sinusoidal acceleration with a constant peak-to-peak value of 3g's covering the frequency range from 10 to 200 hertz without breaking up.

Since one of the applications of the fluid bead memory devices included a visual display, it was of interest to present the bead vibration performance results in contrast with a human tolerance curve, and also with the military specifications for rack mounted missile equipment. Figure C-1 shows the vibration performance envelope for a glycerine bead with gold powder in suspension, coated with organic silica.

In addition a fluid bead undergoing a basic life test in a Zepel coated cylindrical chamber had been cycled 1,660,000 times with no sign of deterioration. The life test set-up for the fluid bead is illustrated in Figure C-2. The switching life of a glycerine bead was found to depend upon a number of factors. Its chemical composition determines the surface tension, density, the maximum amount of humidity allowed in the switching air, the operation temperature, etc. It also depended upon the switching pressure, the surface finish of the memory cell, the geometric shape of the switching path, the surface treatment of the memory cell, and the cleanliness of the surface of the bead. To ensure uniform quality of glycerine based beads, different samples were tested in the same test memory cell. Each treatment of the surface of the memory cell and each coating of the glycerine bead were checked under a microscope to ensure they were free from dust particles. It was found that with reasonable care, the uniformity of the glycerine based beads could be controlled to give reliable performance over the entire test range.

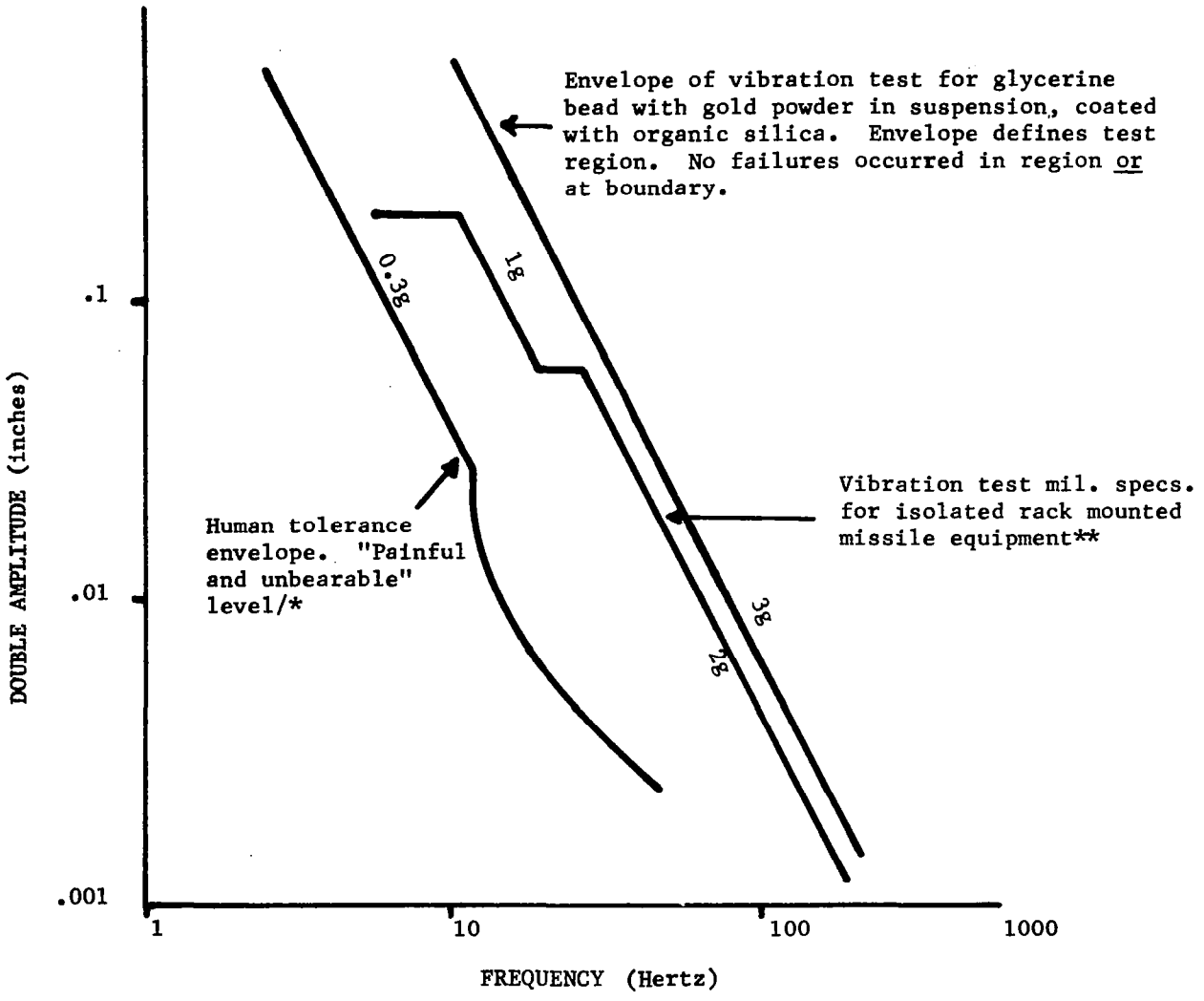

FIGURE C-1 Vibration Test Results of Two-Phase Bead for Use in Fluid Memory Unit

*Hilborn, Edwin H. Handbook of Engineering Psychology. Cambridge, 1965.

**Military Standard Environmental Test Methods for Aerospace and Ground Equipment. MIL-STD-810A (USAF), June 23, 1964.

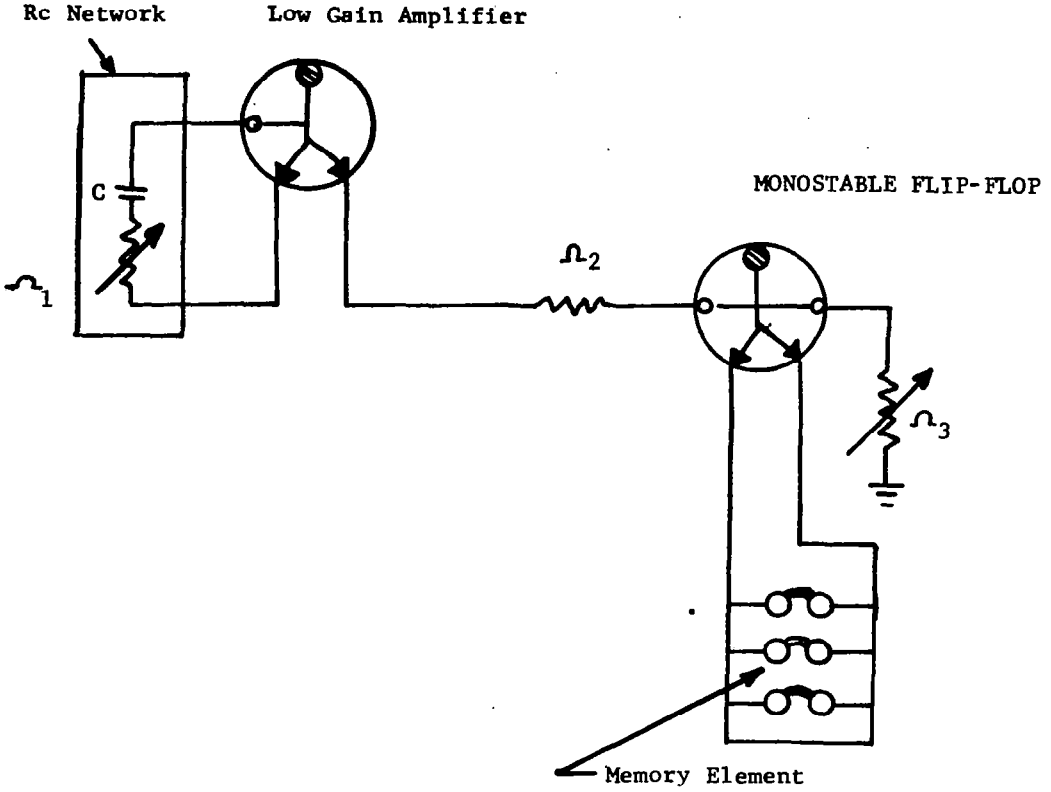

Ω_1 = OSC frequency control resistor

Ω_2 = input impedance of the flip-flop

Ω_3 = Monostable adj. resistor

FIGURE C-2 Pneumatic Oscillator for Life Test of Mercury Memory Element

Appendix D

LOGIC ELEMENT DESIGN

D.1 Design Considerations

In order to meet the requirements of low power and low supply pressure necessary for a demonstration model using a portable blower, it was decided that specially designed fluidic elements would be required. The logical design philosophy was to alternate low gain amplifier/inverters with passive two-input logic elements. The justification for this approach is based on the following assumptions:

1) High gain requires very close tolerance in element dimensions.
2) Multiple fan-out devices are sensitive to variations in the output loads, and therefore require very carefully designed isolators.
3) Low gain elements are capable of operating with very much lower Reynolds numbers than high gain elements using similar aerodynamic phenomena.

A more detailed discussion of some of the factors involved in the design philosophy of fluidic circuits may be found in Reference 1, (page D-12).

D.2 Low Gain Amplifier

The definition of "gain" in this binary system is the pressure ratio between input and output when the control input is in the "ON" state. The average gain for typical loading conditions is 4. Figure D-1 shows the control input and output relationship of the low gain digital amplifier. One important feature of the characteristic curve is that no hysterisis exists. Experience has shown non-hysteretic amplifiers to be faster and more reliable in operation than hysteretic amplifiers when used as logic devices in which the memory feature is not required. Of the series of low gain amplifiers which were designed and tested, the configuration shown in Figure D-2 was incorporated in the final model.

D.3 Logic Elements

There are only two types of passive logic elements used in the logic system: the "AND" gate and the "OR" gate. The dimensions of these elements are shown in Figures D-3(a) and (b); each element is described as follows:

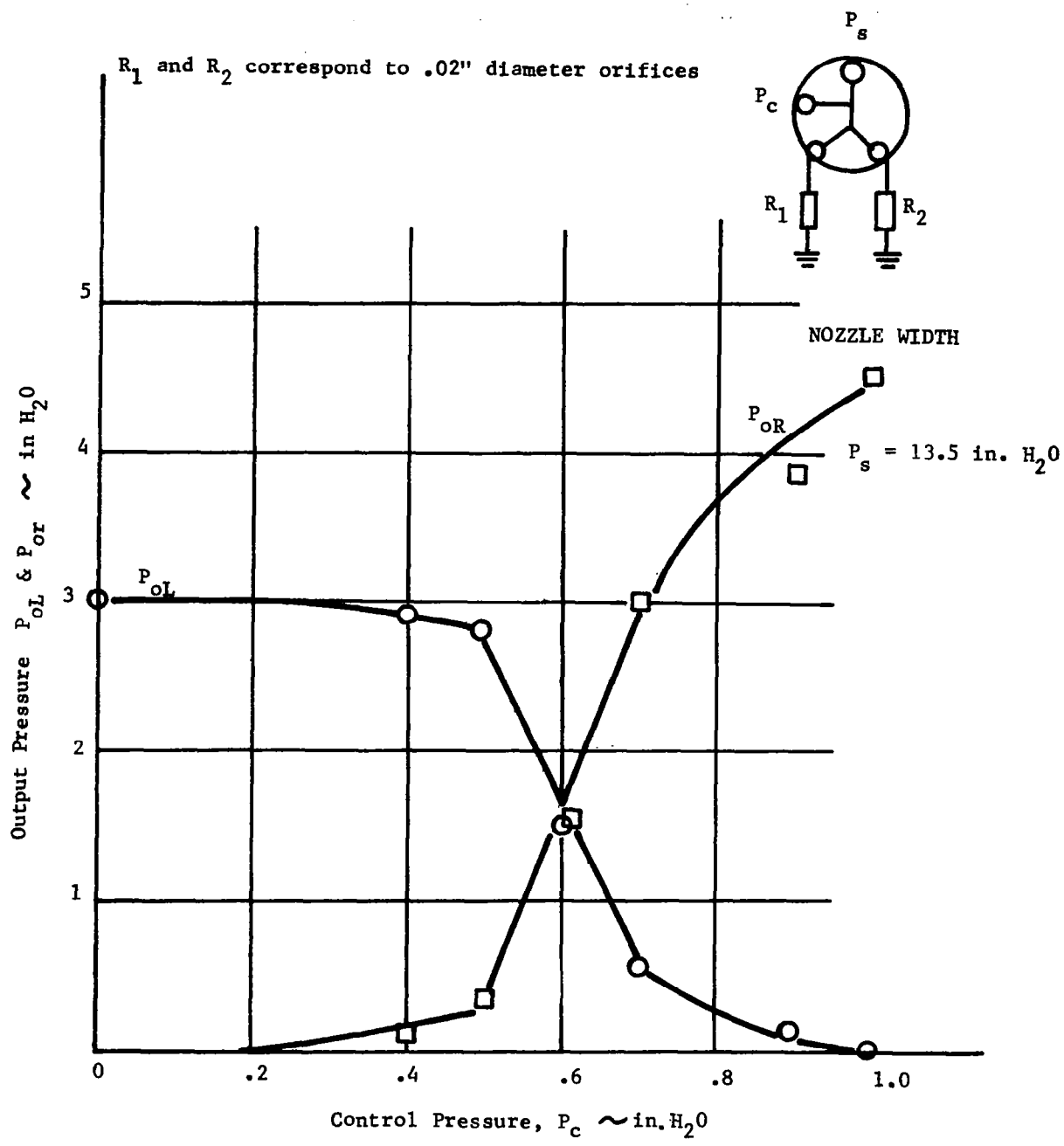

FIGURE D-1 Low Gain Amplifier Characteristic Curve

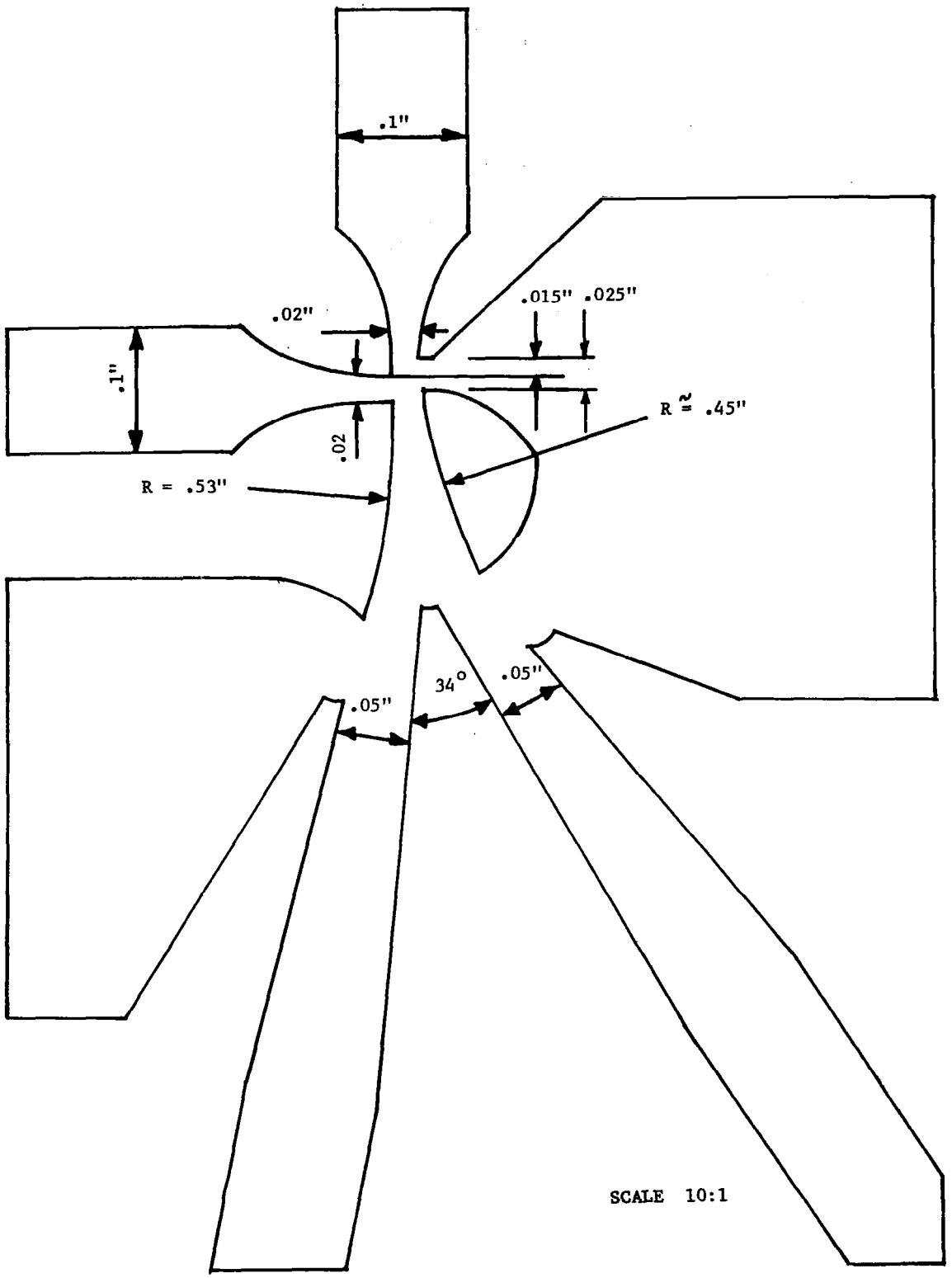

FIGURE D-2 Low Gain Amplifier

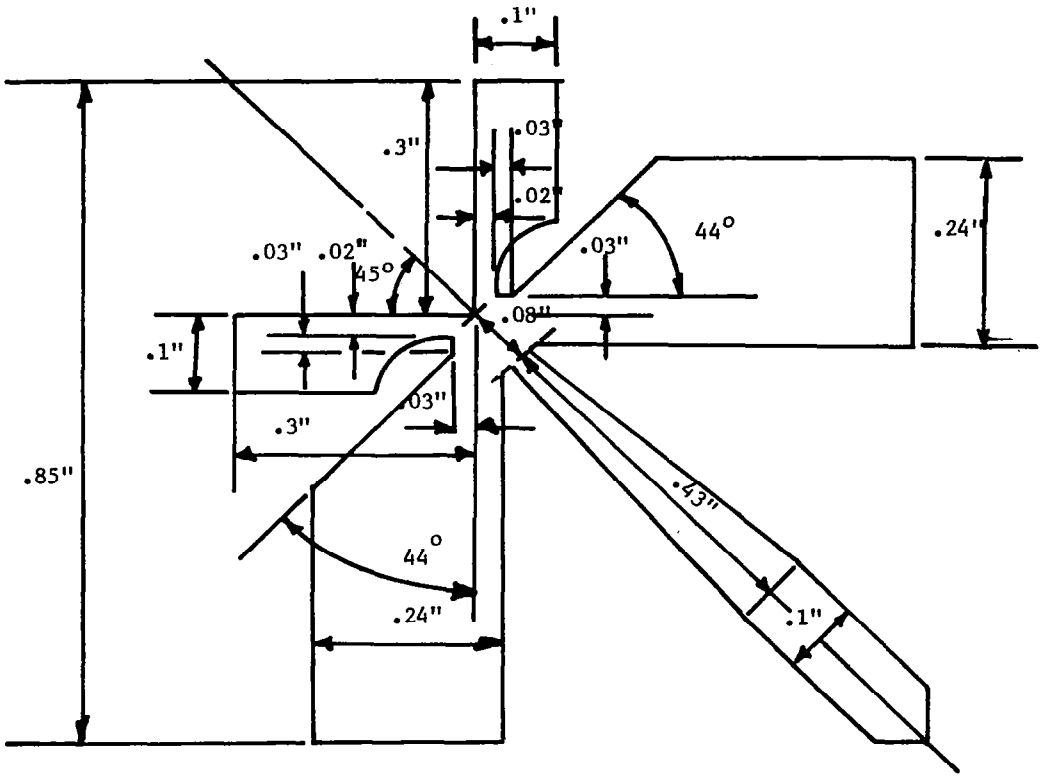

(a) "AND" Gate SCALE 5:1

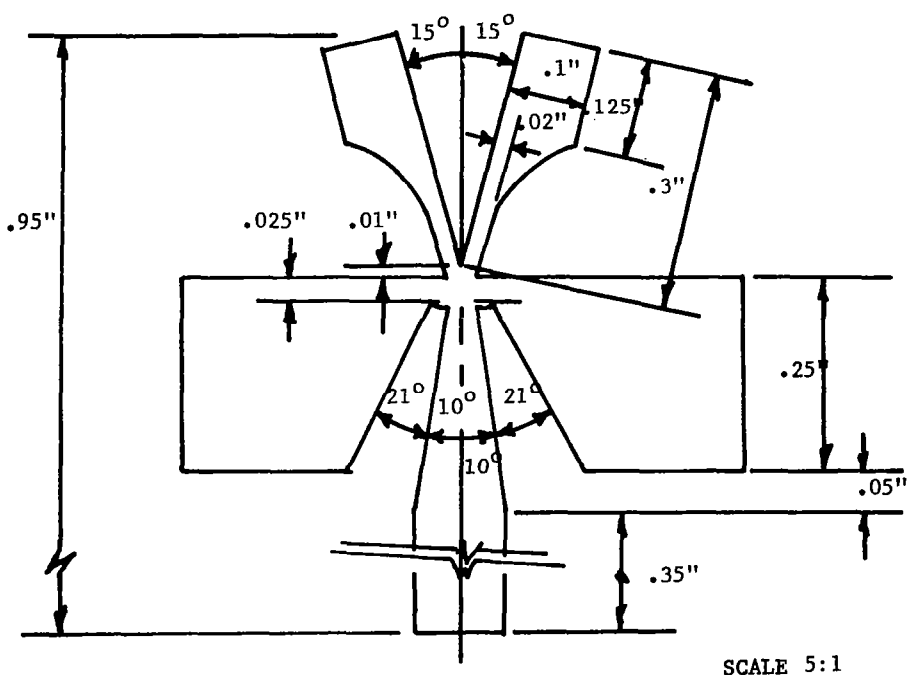

SCALE 5:1

(b) "OR" Gate

FIGURE D-3 Logic Elements

The "AND" Gate

Boolean algebra expression:

$A \cdot B = C$ A, B = input signal

C = output signal

(This standard Boolean notation should not be confused with symbols A through E used to designate columns of cells described elsewhere.) The mathematical equations (Reference 2) used in designing the "AND" gate are:

$$v^2 = v_o^2 \left[1 - \left(\frac{\ddot{y}_e}{K_x}\right)\frac{7}{4}\right]^4 \quad (1)$$

$$V_4 = V_o \quad (2)$$

$$K = 1.378 \frac{b_o}{x_o} \qquad y_{e\ max.} = y_x \quad (3)$$

$$b = (1 - \frac{x}{x_o})b_o \quad (4)$$

$$y = y_e + \frac{b}{2} \quad (5)$$

$$y_b = .169x + .5b_o \quad (6)$$

$$\frac{V}{V_o} = \left[1 - \left(\frac{y_e}{y_{e\ max.}}\right)\frac{7}{4}\right]^2 \quad (7)$$

$$\frac{E}{E_o} = 1 - .182 \frac{x}{x_o} \quad (8)$$

$$\frac{Q}{Q_o} = \left(1 + .364\right)\sqrt{\frac{x}{x_o}} \quad (9)$$

$$x_o = 5.2b_o \quad (10)$$

Equations one to ten apply only to the transition zone of the jet, where:

V_4 = center line velocity

V_o = original nozzle velocity

b_o = throat nozzle width

x_o = length of transition zone

E_o = energy at nozzle

Q_o = flow at nozzle

x = axial distance measured from nozzle

y = distance from the jet center line

y_e = effective value of y

b = core width

w_o = receiver width

y_b = width of jet at end of transition zone

E = energy in jet at distance x from nozzle

Q = flow of jet at distance x from nozzle.

Referring to Figure D-4, the following are the design steps of the "AND" gate:

1) Choose the nozzle width, and nozzle depth. In our model, nozzle width b_o is .02" and depth is .04. (Aspect ratio is 2.) From equation (10) we obtain the transition zone length.

$$x_o = 5.2b_o - .104" \tag{11}$$

2) Determine the minimum receiver width, w_o. By projection of both nozzle widths we obtain w_o, i.e.

$$w_o = 2b_o \cos 45^\circ - 1.4b_o \tag{12}$$

3) Determine the minimum distance d_o. If we assume that only jet A exists, our purpose is to let the whole jet vent into dump (1), so that no air enters receiver. See Figure D-4. From equation (6) we obtain:

$$y_b = .169x + .5b_o = x\tan\phi + .5b_o$$

$$\phi \simeq 10^\circ \tag{13}$$

Therefore, the jet will be bounded between a 20° region on each side of the nozzle. From the intersection of line $\overline{OA}$ and line $\overline{BC}$, we obtain point P, as shown in Figure D-4. Therefore, the distance $d_{o\ min.}$, can be expressed as

$$d_{o\ min.} = \overline{OO'} \tan\left\{\left(\frac{\pi}{2} - \theta\right) + \phi\right\} \tag{14}$$

In this equation, θ is the angle between the nozzle exits and the center line. In our case θ equals 45°; therefore,

$$d_0 = \sqrt{2}\, b_o \tan\left\{45^\circ + 10^\circ\right\}$$

$$= \sqrt{2}(.02\tan 55^\circ) = .04"$$

4) Determine the maximum signal pressure P_A/P_B ratio which can be present without a false indication. The ratio is dependent upon the distance d_o used. In actual design, distance (d_o) should move further down to provide this requirement. In our

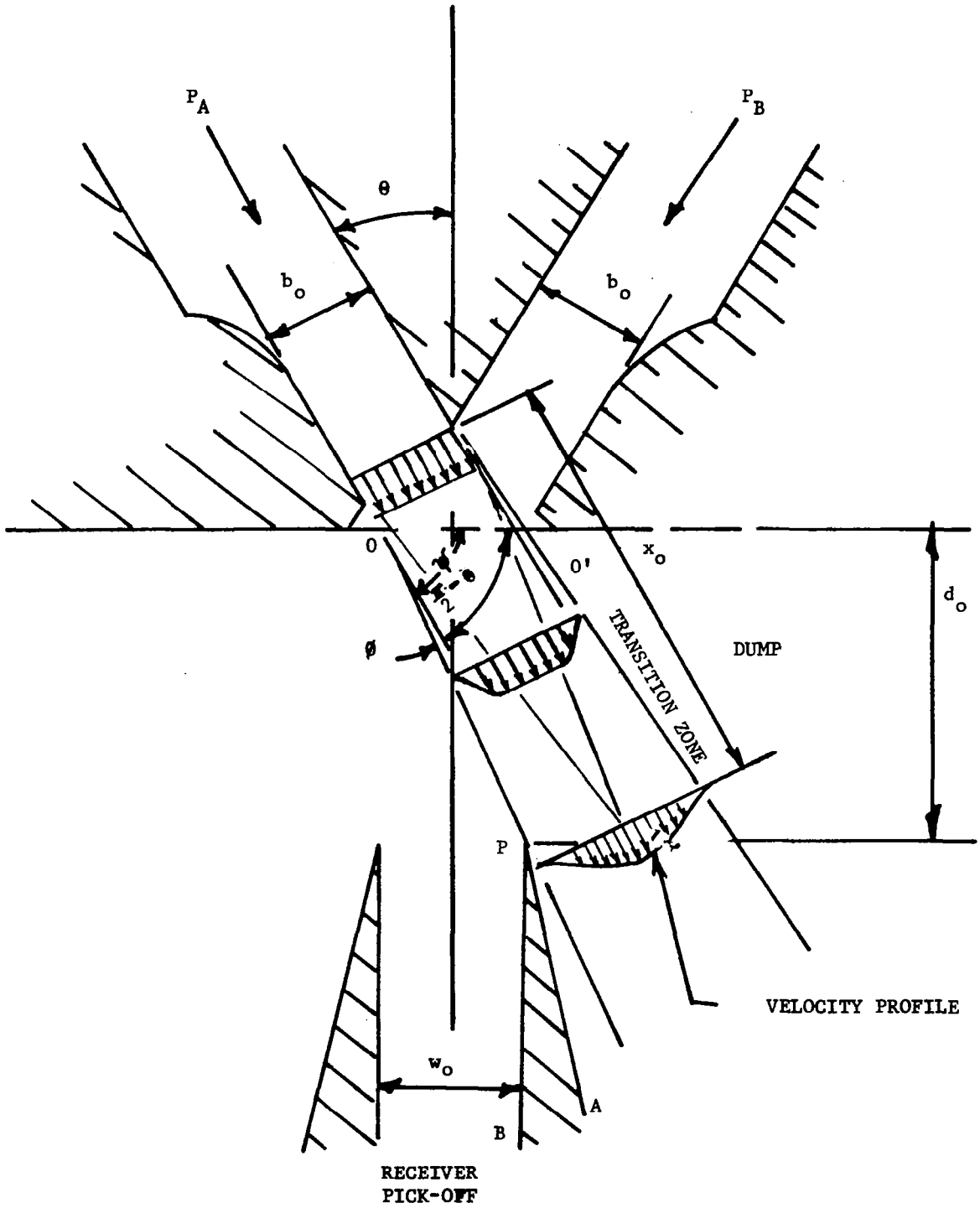

FIGURE D-4 "AND" Gate Design Analysis

design the actual d_o = .06", instead of .04". By equation (14),

$$\tan x = \frac{.06}{2(.02)2} = .212$$

$$x = 65^o$$

The incremental of ϕ is $\Delta\phi = 65^o - 55^o = 10^o$

The question arises as to how much pressure is needed to deflect the power jet from nozzle A to a 10^o angle. From the momentum relation the resultant angle of two impinging jets is

$$\tan \phi = \frac{P_B}{P_A} \quad \text{for} \quad \phi = 10^o$$

$$P_B = \tan 10^o \, P_A = .17P_A \qquad (15)$$

Therefore, if P_A = 3 inches of water, the maximum false pressure of signal $P_{B\ max.}$ is:

$$P_{B\ max.} = 3(.17) = .51 \text{ in. of water}$$

Notice that equation (15) does not consider the jet velocity profile; therefore, actual $P_{B\ max.}$ will be even smaller. In our test result $P_{B\ max.}$ = .5"of water. A reasonable answer can be obtained, therefore, by means of equation (15).

5) Pressure recovery of the "AND" gate is 30% of input signal. Figure D-5 shows the input and output relationship at different load conditions. A linear relation was obtained; therefore we may conclude that scaling laws may be applied over the entire range of pressures tested.

D.4 The "OR" Gate

Boolean algebra expression: A + B = C

The "OR" gate does not lend itself to an analytical treatment since no jet interaction is involved. This element was therefore designed by means of graphic and experimental techniques. Figure D-6 shows characteristic operating curves. The output pressure recovery is between 70 and 80 percent of the input signal when typically loaded.

D.5 "FAN OUT" Unit

The "FAN OUT" unit as shown in Figure D-7(a) is an integrated block

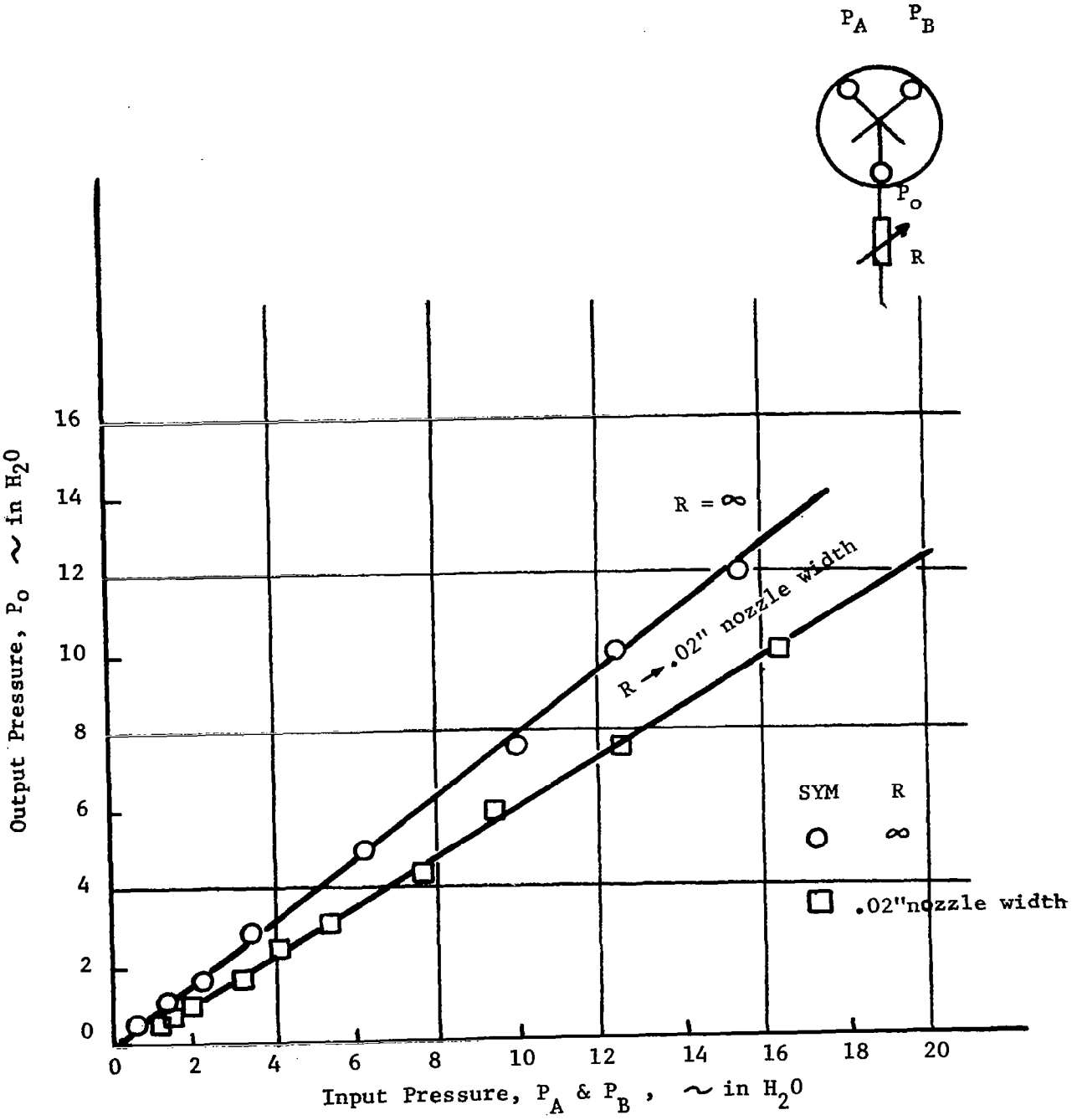

FIGURE D-5 Input & Output Relationship of "AND" Gate

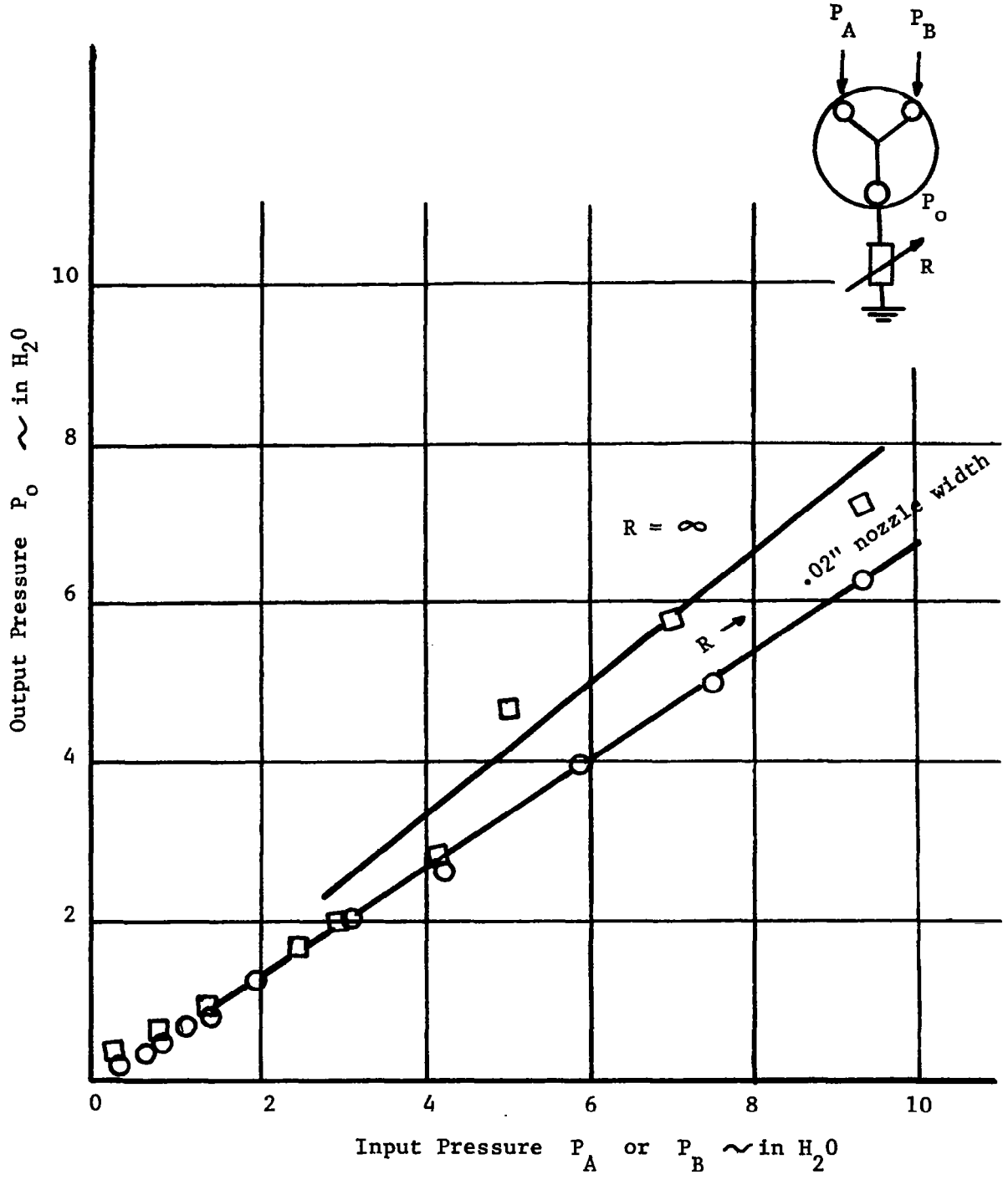

FIGURE D-6 "OR" Gate Characteristic Curve

(a) FAN OUT

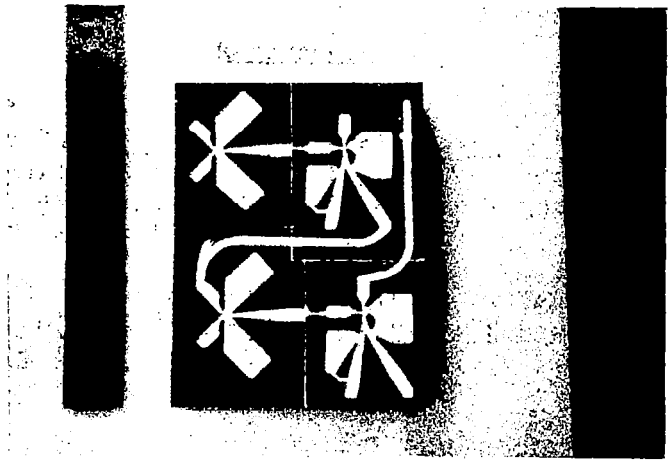

(b) FAN IN

FIGURE D-7 FAN OUT & FAN IN Integrated Unit

consisting of three amplifiers. It has one input and four outputs. The input signal is formed from the memory sensing discriminator, and the output drives the decoding matrix. The function of the "FAN OUT" is no more than a load isolation stage between the memory and decoding systems. Figure D-8(a) shows the characteristic operation curve of "FAN OUT" units.

D.6 "FAN IN" Unit

The "FAN IN" unit as shown in Figure D-7(a) is an integrated block consisting of two "AND" gates and two amplifiers. Its Boolean algebra expression is: $A \cdot B \cdot C = D$. The "FAN IN" unit which has two "OR" gates and two amplifiers can also be used in the decoding matrix system. Its Boolean expression is:

$$\overline{(\bar{A} + \bar{B} + \bar{C})} = D$$

Figure D-8(b) shows the characteristic operation curve of the "FAN IN" unit. The threshold control pressure for a supply pressure of 12 to 23 inches of water, is 0.5 inches.

References

1. Reader, Trevor D. Research and Development in Fluid Logic Elements. Univac Technical Summary Report prepared under contract no. NAS 8-11021 for the George C. Marshall Space Flight Center, Huntsville, Alabama. November 1964.

2. Simson, Anton K. (Massachusetts Institute of Technology) A Theoretical Study of the Design Parameters of Subsonic Pressure Controlled Fluid Jet Amplifiers. Ph.D. Thesis, 1963.

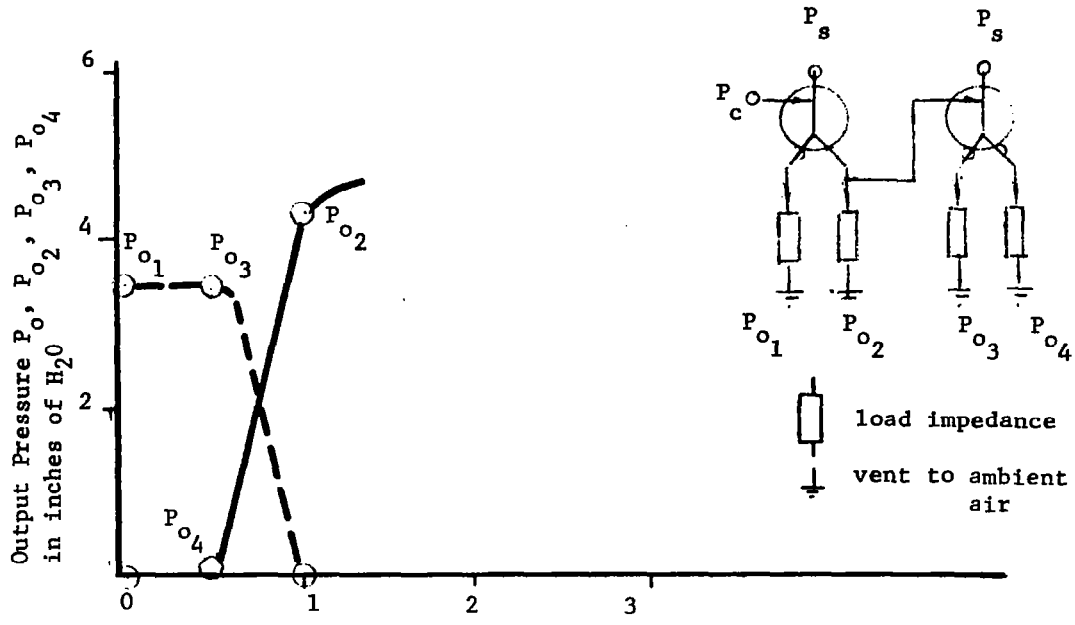

Input Pressure P_c in inches of H_2O

(a) "FAN OUT"

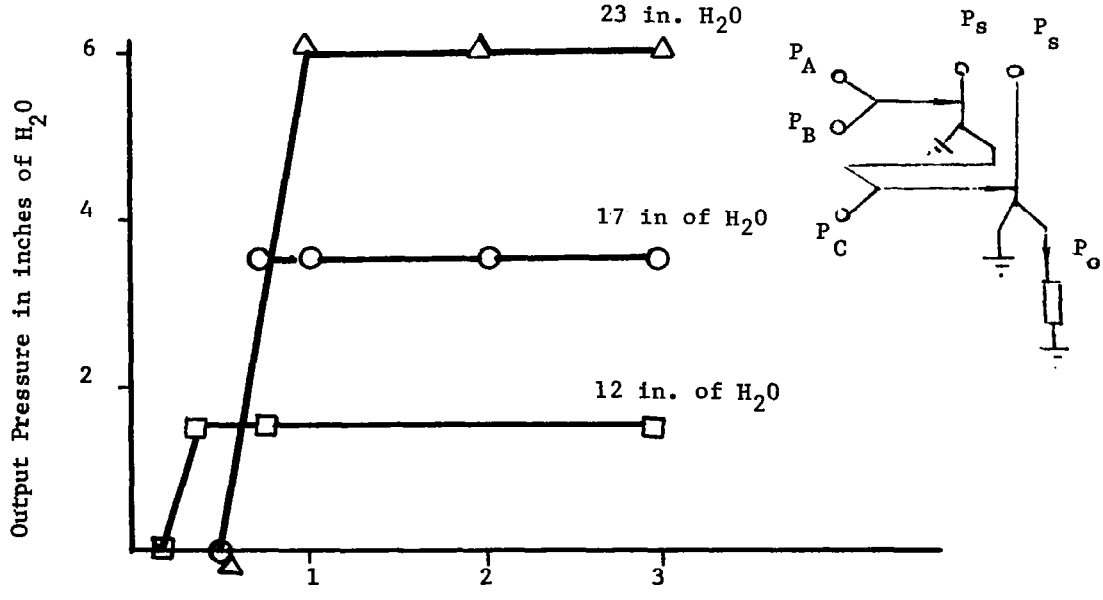

Input Pressure P_A, P_B, & P_C in inches of H_2O

(b) "FAN IN"

FIGURE D-8 "FAN IN" and "FAN OUT" Characteristic Curves

Appendix E

LOGICAL DESIGN OF THE ENCODER

E.1 The Basic Approach

One of the features required of the demonstration model was the ability to store non-destructively and to display eight different alphanumeric characters. In order to obtain eight characters it was necessary to employ three non-destructive memory elements. The decoder converted the eight different combinations of outputs from the three memory elements into unique outputs from eight different channels. Each output channel corresponded to a single alphanumeric character.

The function of the encoder was to fan out from each of the eight decoder outputs to the required number and location of cells in the display panel. Figure E-1(a) shows the pattern of the eight different symbols which were selected for the demonstration model. Figure E-1(b) shows the number of different symbols using each cell. A cell basically is driven by one logic gate, but two or more cells may share one logic gate. For example, cell Aa needs a three input OR logic gate (for symbols "D", "R", and "5"), and cells Bg, Cg, and Dg share one NOR logic gate, i.e. A + R. To simplify the display matrix design, the index of the cells was rearranged in the following sequence: Aa, Ab...Ag, Ba, Bb...Bg, Ca...., Ea...Eg, as shown in Figure E-2. Each column of the display matrix represents a symbol. Each row of the display matrix shows the common cells shared by different symbols, or in other words, the number of inputs to the corresponding logic gates.

E.2 Logical Operations Expressed as Boolean Equations

The outputs of the display matrix are mutually exclusive, therefore by using the dual relationship of Boolean algebra, a two input NAND gate can be substituted for a six input OR gate, etc. Their relationship can be expressed by equations (1), (2), (3), and (4).

$$f = G + C + A + R + D + 5 + 0 = \overline{6} \quad (1)$$

$$f = G + C + A + R + D + 5 = \overline{6 \cdot 0} \quad (2)$$

$$f = G + C + A + R + D = \overline{6 \cdot 0 \cdot 5} \quad (3)$$

$$f = G + C + A + R = \overline{D \cdot 5 \cdot 6 \cdot 0} \quad (4)$$

Also, equations (2), (3), and (4) can be rewritten in OR gate form as:

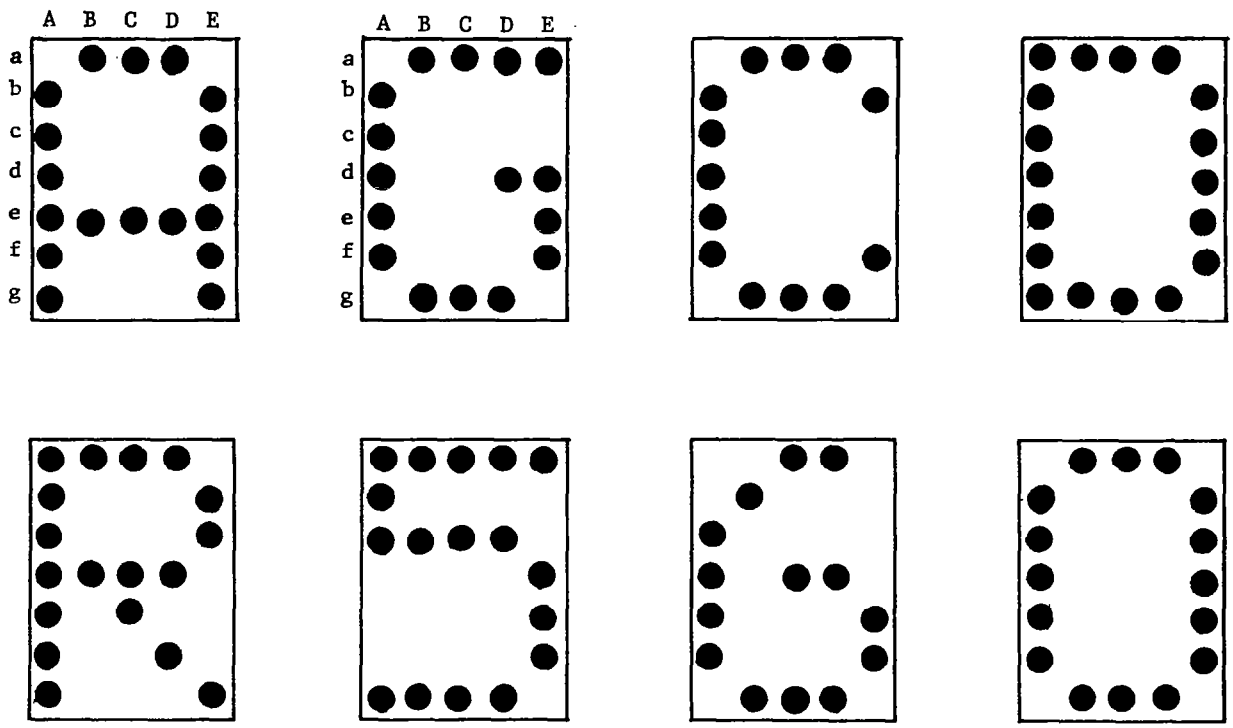

(a) Pattern of Display Symbols

	A	B	C	D	E
a	3	7	8	8	2
b	7	1	0	0	5
c	8	1	1	1	4
d	7	1	2	3	5
e	7	1	2	1	6
f	7	0	0	1	7
g	4	6	6	6	3

NO. indicates the number of different symbols corresponding to each cell.

(b) Display Panel Index

FIGURE E-1

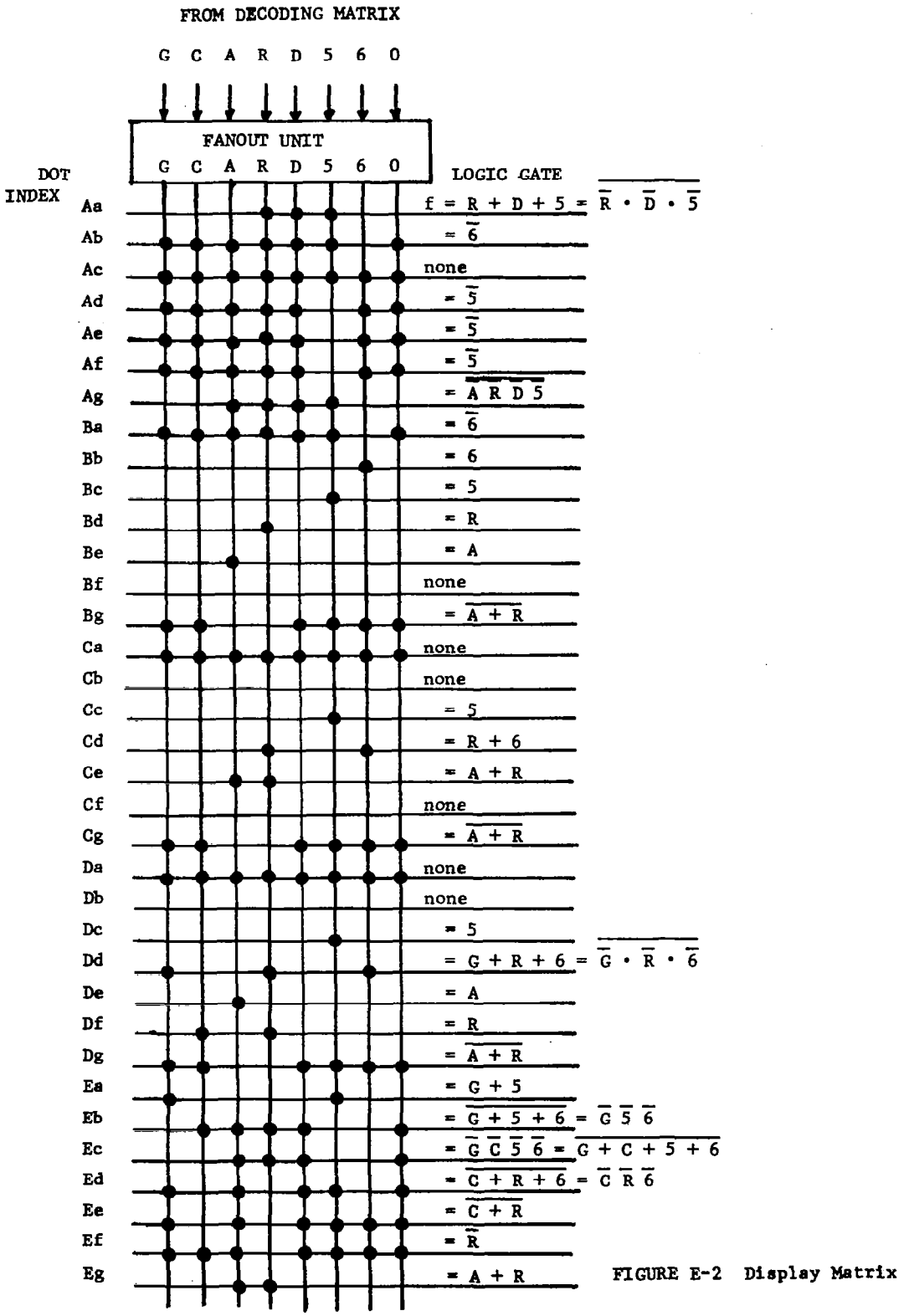

FIGURE E-2 Display Matrix

$$f = \overline{6 \cdot 0} = \bar{6} + \bar{0} \quad (5)$$

$$f = \overline{6 \cdot 0 \cdot 5} = \bar{6} + \bar{0} + \bar{5} \quad (6)$$

$$f = \overline{D \cdot 5 \cdot 6 \cdot 0} = \bar{D} + \bar{5} + \bar{6} + \bar{0} \quad (7)$$

By using the simplest expressions given in equations (1) through (7), it was possible to simplify the logical design of the decoder thereby reducing the number of logic elements required to perform a specific function.

The largest number of inputs required for an "OR" or and "AND" gate was four, since a five input gate could always be replaced by a three input gate using equations (3) and (6). Thus the "worst case" fan-in conditions were a four-input "OR" gates or four-input "AND" gates. Typical four-input "OR" and "AND" fluidic test circuits are shown in Figure E-3. Contrary to our initial logical design philosophy, passive elements were cascaded in these circuits with the resulting penalty of low control pressures applied to the low gain amplifiers. Laboratory tests showed that the gain of these amplifiers was sufficient to permit some cascading. Because the pressure recovery from the "AND" gates was higher than the pressure recovery from the "OR" gates, as shown in Figure E-3, our logical design rules were relaxed to permit the use of not more than two cascaded AND gates. This additional freedom resulted in a simplification of the logic circuits and a corresponding reduction in the number of active elements required.

Optimization of the logical design consisted of manipulating the Boolean equations in order to reduce the number of active and passive elements required. This involved maximizing the use of the available amplifier outputs, and simplifying the equations using the duality concept. A list of the simplified Boolean equations and the corresponding fluidic gates required to satisfy them is given in Table 1.

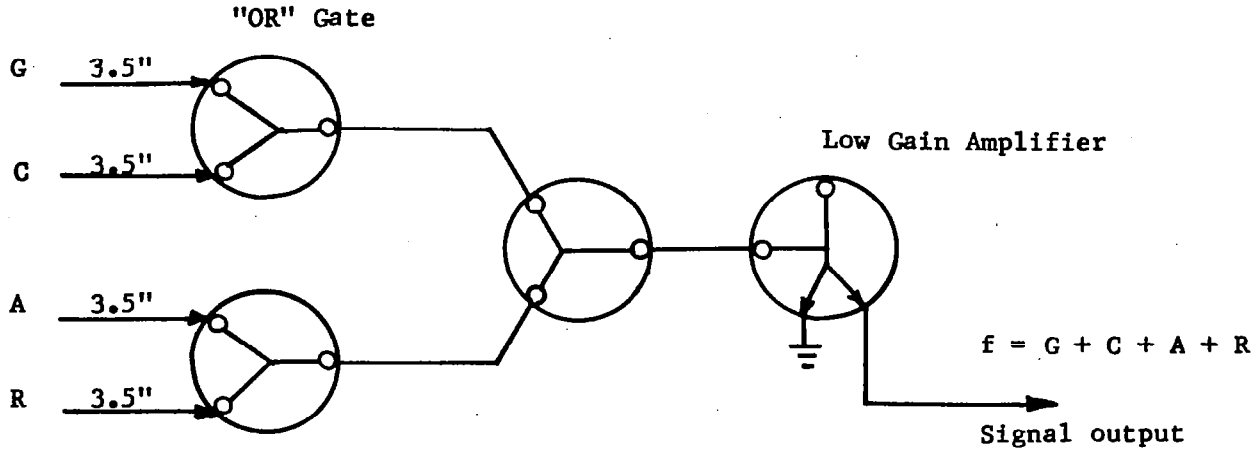

"OR" Logic Circuit

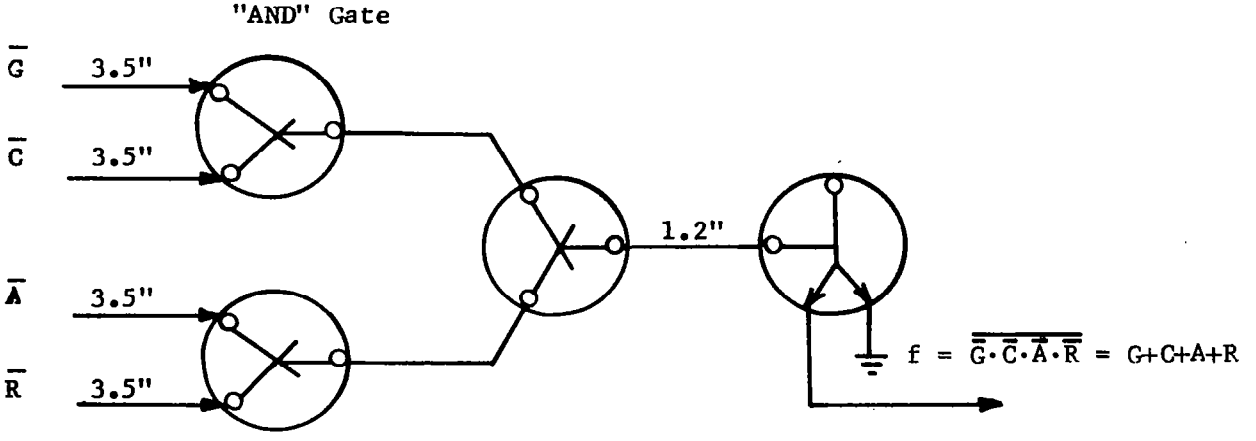

"AND" Logic Circuit

pressure unit: in. of water

symbol ⏚ means vent to air

FIGURE E-3 "OR" and "AND" Logic Pressure Loss Comparison

TABLE 1 Display Matrix Logic Gate Table

CELL INDEX	DISPLAY COMMON SYMBOL	LOGIC GATE	BOOLEAN EQUATION	REMARK
B_b	6	amplifier	$f = 6$	
B_c & C_c & D_c	5	amplifier	$f = 5$	
B_d & D_f	R	amplifier	$f = R$	
B_e & D_e	A	amplifier	$f = A$	
A_b & B_a	A G C D R 5 0	inverter	$f = \overline{6}$	
A_d & A_e & A_f	A G C D R 6 0	inverter	$f = \overline{5}$	
E_f	A G C D 5 6 0	inverter	$f = \overline{R}$	
C_d	R 6	OR	$f = R + 6$	TWO INPUT GATE
C_e	A R	OR; NAND	$f = A + R = \overline{\overline{A} \cdot \overline{R}}$	
E_a	G 5	OR; NAND	$f = G + 5 = \overline{\overline{G} \cdot \overline{5}}$	
B_g & C_g & D_g	G C D 5 6 0	NOR; AND	$f = \overline{A + R} = \overline{A} \cdot \overline{R}$	
A_a	D R 5	OR; NAND	$f = D+R+5 = \overline{\overline{D} \cdot \overline{R} \cdot \overline{5}}$	THREE INPUT GATE
E_g	A G R	OR; NAND	$f = A+G+R = \overline{\overline{A}\ \overline{G}\ \overline{R}}$	
D_d	G R 6	OR; NAND	$f = G+R+6 = \overline{\overline{G}\ \overline{R}\ \overline{6}}$	
A_g	A D R 5	NAND	$f = \overline{A\ D\ R\ 5}$	FOUR INPUT GATE
E_c	A D R 0	NAND	$f = \overline{A\ D\ R\ 0}$	
E_b	A C D R 0	NOR	$f = \overline{6 + 5 + 6}$	THREE INPUT GATE
E_d	A G D R 0	NOR	$f = \overline{C + R + 6}$	
E_e	A G D 6 0	NOR, AND	$f = \overline{C + R} = \overline{C} \cdot \overline{R}$	TWO INPUT GATE
A_c & C_a & D_a	A G C D R 5 6 0	NONE	----------	ALWAYS ON
B_f & C_b & C_f & D_b	NONE	NONE	----------	ALWAYS OFF